Paleoflooding reconstruction from Holocene levee deposits in the Lower Meuse valley, the Netherlands

Peng, Fei; Kasse, Cornelis; Prins, Maarten A.; Ellenkamp, Reinier; Krasnoperov, Maxim Y.; van Balen, Ronald T.

published in
Geomorphology
2020

DOI (link to publisher)
10.1016/j.geomorph.2019.107002

document version
Publisher's PDF, also known as Version of record

citation for published version (APA)
Peng, F., Kasse, C., Prins, M. A., Ellenkamp, R., Krasnoperov, M. Y., & van Balen, R. T. (2020). Paleoflooding reconstruction from Holocene levee deposits in the Lower Meuse valley, the Netherlands. *Geomorphology*, *352*, 1-15. [107002]. https://doi.org/10.1016/j.geomorph.2019.107002

Geomorphology 352 (2020) 107002

Contents lists available at ScienceDirect

Geomorphology

journal homepage: www.elsevier.com/locate/geomorph

Paleoflooding reconstruction from Holocene levee deposits in the Lower Meuse valley, the Netherlands

Fei Peng [a,*], Cornelis Kasse [a], Maarten A. Prins [a], Reinier Ellenkamp [b], Maxim Y. Krasnoperov [c], Ronald T. van Balen [a,d]

[a] Department of Earth Sciences, Vrije Universiteit Amsterdam, De Boelelaan 1085, 1081 HV Amsterdam, the Netherlands
[b] RAAP Archaeological Consultancy, De Savornin Lohmanstraat 11, 6004 AM Weert, the Netherlands
[c] Department of Earth Sciences, Utrecht University, Budapestlaan 17, 3584 CD Utrecht, the Netherlands
[d] TNO - Geological Survey of the Netherlands, Princetonlaan 6, 3584 CB Utrecht, the Netherlands

ARTICLE INFO

Article history:
Received 28 February 2019
Received in revised form 14 December 2019
Accepted 15 December 2019
Available online 17 December 2019

Keywords:
Levee sediments
End-member modelling
Flood Energy Index
Holocene paleoflood

ABSTRACT

This study investigates the Holocene levee deposits and paleoflooding history of the Lower Meuse in the Netherlands based on archeological investigations and sedimentary analyses (grain size, end-member modelling, magnetic susceptibility and thermogravimetric analyses). The levee on the left bank in the study area near Ooijen contains a continuous sedimentary record in the NW downstream part. The archeological evidence and sedimentary results, including a grain size based flood energy index (LFEI), indicate that the Lower Meuse experienced a quiescent flooding period and low sedimentation rates during the mid-late Mesolithic when the levee was low and human influence was minor. Deposition during the Mesolithic shows a fining-upward trend and a highly-developed soil containing abundant artefacts. During the Neolithic and Bronze Age, the flooding intensity was low but gradually increased to a moderate level probably because of deforestation and increased runoff. Limited Bronze Age findings may reflect decreased human activity because of the increased flooding. Starting from the Iron Age, the Meuse experienced a generally enhanced flooding regime, which is reflected by erosion and coarsened sedimentation in the Iron Age and Roman Period. The high peak discharges during the Iron Age may have re-opened a low-lying paleochannel near to the levee during the intensified floods. This general increasing trend is interrupted by the lower flooding phase in the early Middle Ages (Dark Ages). From the middle to the late Middle Ages, the floods intensified again. The coarsening deposition and higher sedimentation rates since the Iron Age resulted from increased floods and higher sediment supply by deforestation and soil erosion. The findings of this study agree with a recent paleoflood reconstruction for the Lower Meuse by using a floodplain archive, implying that levee sediment records have potential in paleohydrological studies if the completeness of the record and chronological information is guaranteed.

1. Introduction

Floodplain sediments are used to study river evolution because they contain information on past flooding regimes, landscape change and human activity (cf. Knox, 2006; Benito et al., 2008; Notebaert and Verstraeten, 2010). Floodplain sediments provide good archives for paleo-hydrological studies, because of their availability, accessibility and completeness (e.g., Kochel and Baker, 1982; Yang et al., 2000; Toonen et al., 2015; Toonen et al., 2017). Wide floodplains, in particular, provide excellent records because they have sufficient space to deposit flooding sediments. Apart from sedimentary archives on floodplains, the reconstructed behavior of river channels may also provide important information on discharge changes. Examples include fluvial planform changes, longitudinal gradient changes, and vertical elevation changes (incision versus aggradation) (Phillips, 2010).

Levees, the connector between the channel and floodplain, however, have obtained relatively less attention in paleoflooding studies. This is because of the more limited sediment preservation potential on levees (Allen, 1965; Brierley et al., 1997), as the sediments on levees can be easily eroded by later channel migration, floods and human-induced river regulation. Also, the small size of levees relative to the wide floodplain may lead to levees being easily disregarded. Finally, levee sediments consist of clastic materials with little organic matter, which hampers AMS ^{14}C dating and often produces unreliable OSL dating results because of insufficient exposure prior to burial (Duller, 2004; Brook et al., 2006; Fuchs and Owen, 2008; Cunningham and Wallinga, 2012; Zhao et al., 2018). Consequently, levee sediments are commonly not used in paleohydrological studies.

* Corresponding author.
E-mail address: f.peng@vu.nl (F. Peng).

https://doi.org/10.1016/j.geomorph.2019.107002
0169-555X/

However, like floodplain sedimentary archives (e.g., Toonen et al., 2015; Peng et al., 2019), the alternating coarser and finer levee sediments can in principle be used to infer flooding regime changes, if other factors (i.e., tectonic movements, channel migration and incision) can be ruled out or constrained by additional data. The relative contributions of finer and coarser deposits can be determined by performing end-member modelling analysis on grain size distributions in vertical sections (e.g., Toonen et al., 2015; Peng et al., 2019). End-member modelling analysis has been successfully applied to the various sedimentary systems, including floodplain deposits, to understand their source, transport mechanism and depositional environment (i.e., Weltje and Prins, 2003; Prins et al., 2007; Toonen et al., 2015; Peng et al., 2019). These studies indicate that the end-member modelling approach is capable of distinguishing the different contributing components that reflect the corresponding depositional processes. In fluvial environments (floodplains and levees), a large proportion of coarse end members reflects high discharges, whereas large amounts of fine end members can be associated with low floods, and sometimes with intense soil formation (as a result of strongly reduced sedimentation rates). In addition, long-term human occupation of a levee may also reflect a phase of lower flooding magnitudes, and therefore such archeological information can be combined with inferences from the sedimentary grain size record.

By far, most detailed sedimentological and geomorphological studies on levees have been conducted in the North American river basins (e.g., the Mississippi River in the USA, the Saskatchewan and Columbia rivers in Canada) and the Tuross River in Australia (Fisk, 1944; Fisk, 1947; Wolman and Leopold, 1957; Farrell, 1987; Smith et al., 1989; Ferguson and Brierley, 2002). According to Brierley et al. (1997), levees have the following four characteristics: (i) they are proximal to channel margins; (ii) they have a triangular cross section; (iii) they are ribbon-like, elongated, and aligned parallel to the channel; (iv) their highest elevation is at or close to the edge of the channel, and the elevation slopes away toward floodplain. However, these key geomorphological and sedimentary attributes of fluvial levees show remarkable variability even within the same river system. For instance, in the Lower Meuse valley in the Netherlands, the development of the levees depends on the tectonic setting. Levees are well developed and can easily be distinguished on the uplifting Peel Block and subsiding Venlo Block (Fig. 1A) because of limited lateral channel migration during the Holocene (Kasse et al., 1995). Therefore, long-term vertical aggradation could occur on the levees. However, in the subsiding Roer Valley Graben (Fig. 1A), located farther upstream, the levees are generally lower because of the high rates of lateral channel migration that have eroded pre-existing levee sediments.

In this study we analyze the sedimentological and archeological record of a well-developed Holocene levee, located along the Lower Meuse River, on the Venlo Block. Three vertical sections, located in a man-made trench perpendicular to the levee, were continuously sampled and analyzed. We integrate the chronological framework offered by archeological surveys with the sedimentary analyses (grain size, end-member modelling, magnetic susceptibility and TGA analyses). The main objectives of this study are to discuss the feasibility of levee sediments for paleoflood reconstructions, to determine the flooding regime during each cultural period since the late Mesolithic, and to compare the flooding results of this study to those obtained previously in a floodplain setting about 9 km downstream (Peng et al., 2019).

2. Research area

The Meuse originates in northeastern France, flows through the uplifting Ardennes and subsiding Roer Valley rift system, and finally debouches into the North Sea. It has a length of 900 km and a catchment area of 33,000 km^2. As a rain-fed river, the annual average discharge of the Lower Meuse is about 230 m^3/s. In the Roer Valley rift system, the Meuse passes through the subsiding Roer Valley Graben, and the uplifting Peel Block and subsiding Venlo Block (Fig. 1A; Van Balen et al., 2005) before turning to the west in the Rhine-Meuse delta and finally flowing into the North Sea. The study area is located along the Lower Meuse near Ooijen in southeastern Netherlands, and lies on the Venlo Block, in the transition area from a narrow floodplain setting (uplifting Peel Block) to a wider floodplain setting (relatively subsiding Venlo Block; Fig. 1A). Bounded by the Late Pleniglacial terraces in the west and Younger Dryas dunes in the east, the landforms in-between are mainly comprised of river terraces and floodplains that formed in the Late Glacial (Bølling, Allerød and Younger Dryas) and Holocene (Kasse et al., 1995).

During the transition from the Late Glacial to the Holocene, the Meuse changed from a braided river with higher peak discharges to a meandering river system with lower peak discharges in response to climate amelioration (Kasse et al., 1995; Huisink, 1999; Tebbens et al., 1999). This river morphological transition resulted in channel abandonment. The abandoned and buried braid channels can be identified on the LIDAR imagery and are referred to as (Ooijen Abandoned Channels) OAC-1 and OAC-2 (Fig. 1C) in this study. At the start of the Holocene the Meuse changed to a low-sinuosity meandering river. The river has experienced very little lateral migration in the course of the Holocene and hence high levees have formed in this area (Kasse et al., 1995). The investigated part of the levee is located next to the present-day Meuse, on the NW part of the point-bar near Ooijen (Fig. 1C). The elevation of the present river channel is 10.7 m (+NAP), and the highest part of the levee reaches to 15.5 m (+NAP) in the SE and decreases to 14.6 m (+NAP) in the NW (Fig. 1D).

3. Materials and methods

3.1. Location selection, archeological investigations and sampling

To control future flooding events in the Lower Meuse valley, the floodplains and river banks have been and will be lowered. Prior to the digging activities, a series of archeological investigations have been carried out in the last two decades in the Well-Aijen and Ooijen-Wanssum areas (Fig. 1A, B; and see Isarin et al., 2017 and references therein). The main goals of these investigations were to reconstruct the paleoecological and paleogeographical developments, and to trace prehistoric human activity. The chronological framework was based on artefacts (mainly flint and pottery) typology, combined with OSL and ^{14}C dating (Ellenkamp et al., 2018).

In 2016, a project (code: OOYWA2) was carried out near Ooijen (Fig. 1C, center coordinate: 51.51° N, 6.16° E). Boreholes, cross sections and trenches were drilled and excavated in the levee. The results from these investigations (Ellenkamp et al., 2018), including the lithostratigraphical subdivision and chronology based on cultural periods, were used in this study. We also adopted the labelling of the seven units. The samples for sedimentary analysis were obtained from three vertical sections in trench-57, located close to the northwestern tip of the levee (transect 2 in Fig. 1C). We did not take samples in trench-41 (transect 3 in Fig. 1C), located near the central part of the levee because this trench was no longer available for sampling. However, the stratigraphical information from this trench is also described below, based on Ellenkamp et al. (2018), because it provides useful information about the general evolution of the levee. The lengths of the three sampled vertical sections in trench-57, sections A, C and B, are 256 cm, 230 cm and 204 cm, respectively. Based on the results of the archeological investigations, the three sections are semi-continuous and span approximately the last 10,000 yr of the Holocene period (from the Mesolithic to modern time). The sampling resolution adopted in the vertical sections is 2 cm. This interval is approximately equal to 100 yr of sedimentation, which we consider to be a resolution suitable to determine flooding phases on a centennial and millennial time-scale.

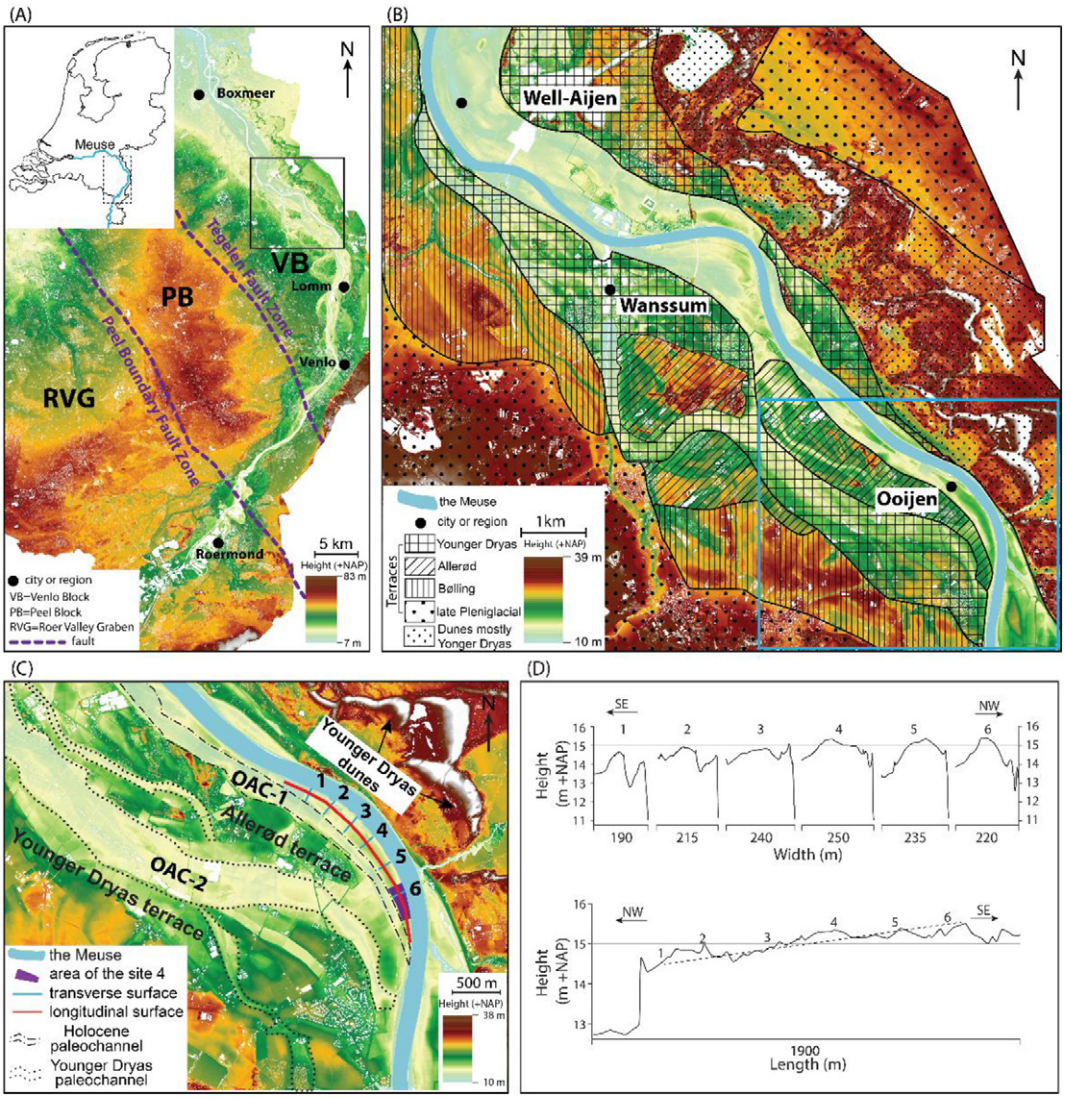

Fig. 1. (A) Digital elevation map (DEM) of the southeastern Netherlands with Lower Meuse (dashed box in the insert) and the tectonic blocks. The uplifting Peel Block (PB) is separated from the subsiding Venlo Block (VB) and Roer Valley Graben (RVG) by fault zones (Van Balen et al., 2005). The light-green area depicts the distribution of the Holocene floodplain, from which it shows a narrow floodplain on the PB, that gradually widens at the VB. Solid box shows the study area (Ooijen). (B) DEM including the Ooijen and Well-Aijen, Late Glacial and Late Pleniglacial terraces (after Kasse et al., 1995). The light-green area along the Meuse River is the Holocene floodplain. Blue box delineates the Ooijen area depicted in (C). (C) DEM of the study area near Ooijen. The dashed lines outline the abandoned channels including OAC-1 and OAC-2. OAC-1 separates the investigated levee from the Allerød terrace. West and East of the Meuse, Late Glacial terraces and Younger Dryas dunes are present (Kasse et al., 1995). Red line shows the convex part of the levee, and six transects were chosen to show the morphology of the surface. The locations of trench-41 and trench-57 are situated at transects 3 and 2 of the levee, respectively. The purple area depicts a previous archeological site (site 4, see Section 5.1). (D) The topographic transects perpendicular (upper diagram) and parallel to the levee (lower diagram). The levee at transect 6 is ~0.9 m higher than the levee at transect 1.

3.2. Magnetic susceptibility (MS)

The mass-specific MS (χ) was measured using an Agico Multi-function MFK1-FA Kappabridge in the paleomagnetic laboratory at Utrecht University. All the measurements were carried out with a frequency of 976 Hz.

In previous decades, a large volume of papers has reported the MS records of loess, lacustrine and marine sediment sequences (e.g., Thompson et al., 1975; An et al., 2001; Litt et al., 2001; Vandenberghe et al., 2004; Lee et al., 2008; Ao et al., 2010; Herb et al., 2013). The correlation between MS variations and other lithological and geochemical proxies (like grain size composition, soil layers and isotope data) is widely used in paleoclimatology, but few MS records for Holocene fluvial levee sediments have been reported up to now. Variations of MS in levee sediments might reflect changing fluvial transport and/or sediment source conditions, and can also represent local soil formation.

3.3. Thermogravimetric analysis (TGA)

Thermogravimetric analysis is used to obtain the loss-on-ignition (LOI) (Heiri et al., 2001) for each sample. The analysis is performed on a Leco TGA701 analyzer at Vrije Universiteit Amsterdam. The mass loss of each sample was obtained in a process of stepwise heating from room temperature to 1000 °C to obtain the organic matter fractions. We used the LOI_{550} (loss-on-ignition at temperature 550 °C) to determine the total organic matter content (TOM) in this study. Organic matter content can provide information on the maturity of the soils (Boyle, 2004; Santisteban et al., 2004).

3.4. Grain size analysis and end-member modelling

The method described by Konert and Vandenberghe (1997) was used for sample preparation prior to grain size analysis. For each sample, 10 ml 30% H_2O_2 and 5 ml 10% HCl was used to remove organic

matter and calcium carbonates, respectively. After pretreatment, grain size distributions (GSDs), ranging between 0.1 and 2000 μm, were measured with a Sympatec HELOS KR laser-diffraction instrument at Vrije Universiteit Amsterdam. The grain size analysis resolution is 2 cm for sections A and B, and 4 cm for section C.

We used end-member modelling to decompose the whole GSDs dataset from the three sampled sections into a series of end members. The end members can be interpreted in terms of sediment source, transport and deposition, which cannot be identified using univariate grain size parameters alone (Prins et al., 2007; Van Hateren et al., 2018). Here, we applied the AnalySize end-member modelling package (Paterson and Heslop, 2015). A class-wise r^2 was used to determine the minimum number of end members needed to adequately describe the GSD dataset (Paterson and Heslop, 2015; Van Hateren et al., 2018). The end-member mixing coefficients are used to determine the temporal flood energy variability by calculating an end-member ratio that highlights variability in the coarse end of the grain size distributions, i.e., the bedload component of the levee sediments.

3.5. Chronology

The sediments in trench-57 are mainly composed of sand, silt and silty clay. No organic macro remains suitable for ^{14}C dating were observed. Meanwhile, the clastic materials used for OSL dating have systematically produced ages that are too old and contradictory to the obtained archeological information (Ellenkamp et al., 2018). In this context, we constrain the chronological framework to archeological periods. We define the formation time of each unit to archeological periods rather than constructing a conventional radiometric-dating-based chronology model. The stratigraphic position of the archeological remains from each subunit horizon and ^{14}C dating information from adjacent trenches in the same levee (Ellenkamp et al., 2018) played important roles in constraining the ages of the different units. Chronological information (the start and end of each unit) from subunit 4Ab upwards is derived from archeological results (Ellenkamp et al., 2018). The age interval for each archeological period is based on the Table 4.1 from Ruijters et al. (2017). The ages of underlying subunits 4C and 4BC are inferred from the stratigraphic relationships and a previous paleochannel study (OAC-1) (Tebbens et al., 1999).

4. Results

4.1. Geomorphological analysis

A digital elevation map (DEM) of the study area, and its interpretation, are shown in Fig. 1B and C. The levee has a SE-NW orientation and its total length is ~1.9 km (Fig. 1C, D). The DEM and six cross-sectional topographic plots show a general slope of the crest of the levee of 0.092 m/m to the NW (Fig. 1C, D). In a transverse direction (SW), the topography of the levee has a minor slope of 0.012 m/m (Fig. 2). To the SW of the levee, an old channel (OAC-1) separates the investigated levee from the Allerød river terrace (Fig. 1C). This channel was abandoned in the early Holocene (Tebbens et al., 1999). Farther to the west another abandoned channel (OAC-2) is present (Fig. 1C). This channel incised into the Younger Dryas terrace; it was abandoned at the end of the Younger Dryas (Kasse et al., 1995). However, because of the low elevation of channel OAC-2, it may have functioned as a secondary channel during high floods in the Holocene. With the three sampled sections, trench-57 is located near the northwestern end of the levee (transect 2; Fig. 1C, D), in a relatively low position, which provided optimal conditions for completeness of the sedimentary record.

4.2. Stratigraphic descriptions and sedimentary results

Generally, the sedimentary sequence (in trench-57) shows a homogeneous structure, without visible flood laminae. The levee deposits in trench-57 have been grouped into seven sedimentary units (Ellenkamp et al., 2018). The subdivision is based on sediment texture, soil structure and color. Most units were subdivided into 2–3 subunits based on soil characteristics (Ellenkamp et al., 2018) (Fig. 2). The vertical and lateral variations of MS, TOM and median grain size in the vertical sections combined with the stratigraphic subdivision are shown in Fig. 3. The GSDs of each unit have similar characteristics in the three sampled sections.

End-member modelling results show that a four-end-member model is capable of explaining >95% of the total grain size variation (Fig. 4a), and its performance is consistently high throughout the dominant size range (Fig. 4b). EM1 has a primary mode at 60 μm and a secondary mode at 5 μm. EM2, EM3 and EM4 all have a unimodal distribution, with modes at 230 μm, 420 μm, 840 μm, respectively (Fig. 4c). We also decomposed the GSDs into five, six and seven end

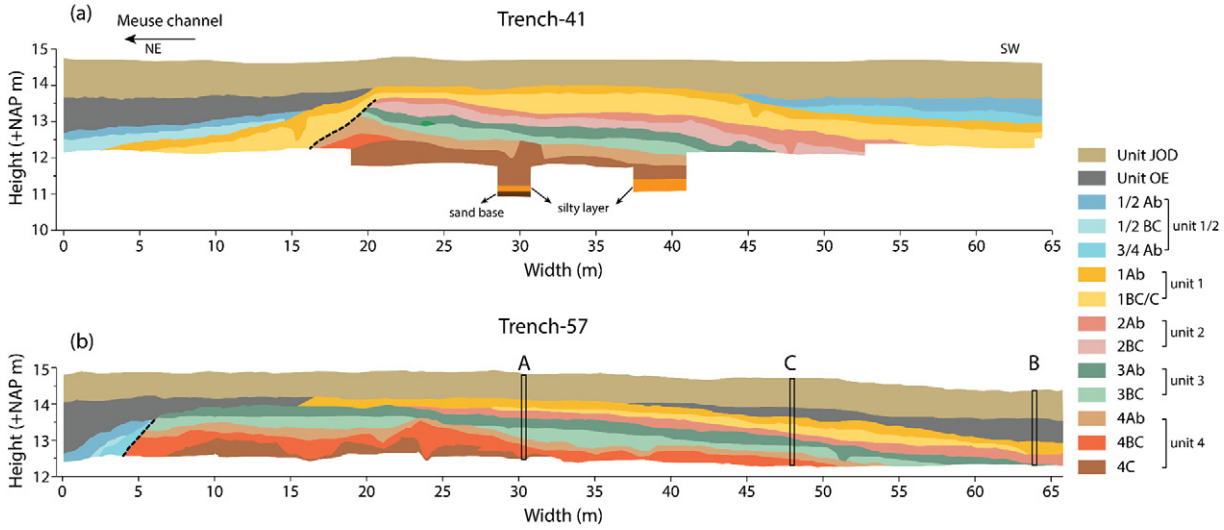

Fig. 2. Seven units are shown in the stratigraphical profiles of trench-41 (a) and trench-57 (b). The vertical bars in (b) signify the positions of the sampled sections A, C and B. Trench-41 and trench-57 are situated at transects 3 and 2 of the levee (Fig. 1C), respectively. Please refer to Table 1 for archeological periods. Dashed lines show the erosional contact. NAP = Amsterdam Ordnance Datum.

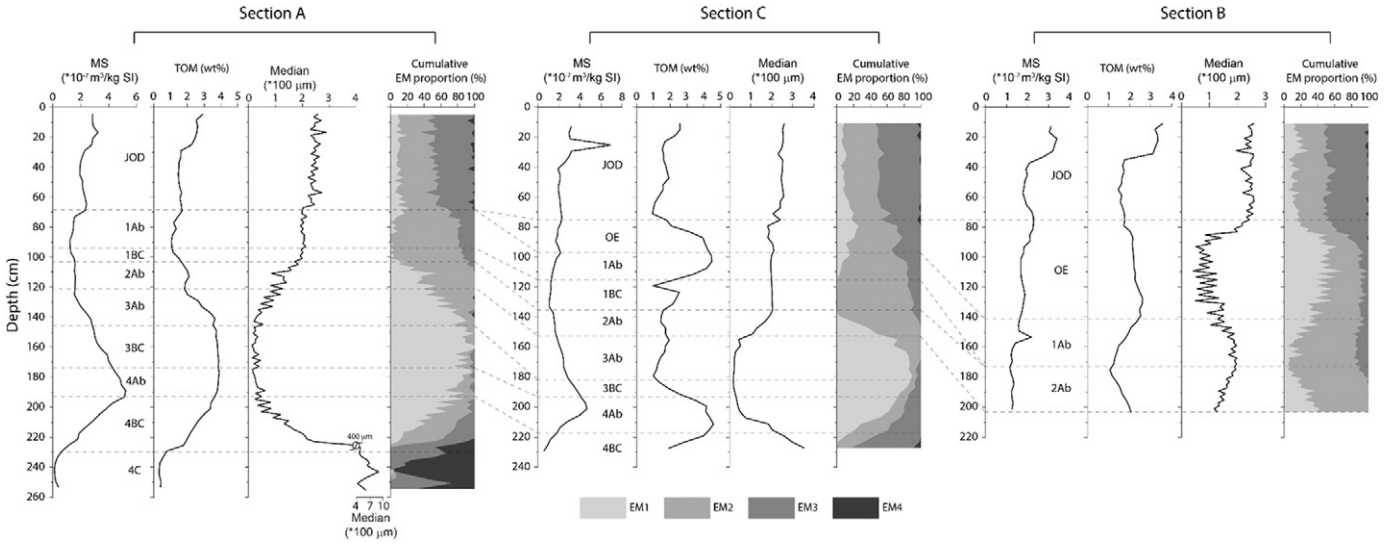

Fig. 3. Sedimentary characteristics of the three sections. For each section, the magnetic susceptibility (MS), total organic matter (TOM), median grain-size and the cumulative end-member (EM) proportion records are shown from left to right. Note a cut-off at 400 μm in the median grain size curve in section A. The EM proportions are derived from the EM modelling analysis. The dashed lines show the correlation of the units in the sections. Sampling in section B starts from 2Ab subunit upwards. The OE unit is missing in section A and well developed in section B.

members. These models show that EM1 cannot be further decomposed by increasing the number of end members. A clear feature of the results is that, in each section, the variation of fine EM1 roughly parallels the MS and TOM variations (Fig. 3) and has an opposite relation to the median grain size variation.

4.2.1. Very coarse sand and clay deposits at the base

The basal sand and clay sediments were only exposed in trench-41 (Fig. 2a), which was no longer available for sampling; they were not encountered in trench-57 because of a high groundwater level. The sediments are yellow-brown, poorly sorted and consist of silty clays overlying the very coarse sands. Grain size and MS analyses were not performed for these sediments. Below we describe the sedimentary results (MS, TOM and grain size) in the framework of the archeological subdivision because the variations of the sedimentary characteristics largely coincide with the archeological subdivision.

4.2.2. Unit 4 (4C-4BC-4Ab)

Unit 4 has the largest thickness and has been well preserved in the center of the levee (section A); it thins toward the western part of the trench (Fig. 2). This unit was not exposed in section B because of the high groundwater level.

This unit consists of three subunits with different colors and textures (Fig. 5a). Subunit 4C features a clearly horizontally layered structure (Fig. 5a) and consists of brown-yellow, rusty sand deposits. Small shell fragments were observed in this subunit. The MS and TOM in 4C are very low, about 0.2×10^{-7} m^3/kg and 0.3 wt%, respectively, and the median grain size varies between 400 and 850 μm. Subunits 4BC and 4Ab show dark brown colors and a homogenous structure indicating soil formation (Fig. 5a). In section A, the MS and TOM show a consistent increase from 0.6 to 5×10^{-7} m^3/kg and from 0.7 to 4 wt% in 4BC, respectively. Subsequently, the MS drops slightly while the TOM remains unchanged in 4Ab. In section C, the TOM shows a different behavior in 4Ab where it drops after reaching high peak values (4 wt%). The median grain size rapidly decreases to ~20 μm in the two subunits (Fig. 3).

Overall, unit 4 shows a fining-upward trend in sections A and C, (Fig. 3). This is reflected by the median grain size record, but even more clearly by the end-member modelling results: the coarse end member EM4 is only dominant in subunit 4C, whereas the proportion of the finest end member, EM1, steadily increases upwards to 90% in 4Ab (Fig. 3). In addition, the grain size compositions in sections A and C show a synchronous variation (Fig. 3); there is no clear lateral grain size change, indicating vertical aggradation on a levee setting, instead of, for example, deposition by lateral point-bar migration. Subunit 4Ab is the oldest sedimentary layer in which early-middle Mesolithic archeological remains have been found.

4.2.3. Unit 3 (3BC-3Ab)

Unit 3 differs from the underlying unit 4 by its brownish and darker color and densely distributed small burrows indicating soil formation during deposition (especially in subunit 3BC, Fig. 5b). This unit contains finer sediments (silty clay, featuring a soil layer) and was not exposed in section B. This unit is subdivided in two subunits, 3BC and 3Ab. Subunit 3BC has a brown color and 3Ab shows a slightly darker color (Fig. 5b, c). The sediments exhibit a homogenous structure and no laminae were observed. Subunit 3Ab has recognizable charcoal spots (not shown here) that were rarely observed in underlying subunit 3BC. Hence, subunit 3Ab was used as a "guide layer" for correlation during the field investigation.

In sections A and C, the MS decreases upwards steadily from ~4.0 to 1.8×10^{-7} m^3/kg (Fig. 3) while the TOM records show different patterns. In section A, the TOM value remains high (~3.7 wt%) in subunit 3BC and decreases to 1.9 wt% in subunit 3Ab, but in section C the value decreases sharply (from 4.6 to 1.1 wt%) in subunit 3BC and rises to 1.7 wt% in subunit 3Ab (Fig. 3). The median grain size has little variation in 3BC but begins to increase gradually to 100 μm in 3Ab in sections A and C (Fig. 3). Corresponding with a coarsening-upward trend, the dominant very fine EM1 in subunit 3BC gradually decreases to about 40% in subunit 3Ab, and the contribution of coarser EM2 rises to around 45% (Fig. 3). In the whole unit the proportion of EM3 is very limited (<10%).

4.2.4. Unit 2 (2BC-2Ab)

In the field, unit 2 was distinguished from the underlying clay-rich subunit 3Ab by its sandy composition (Fig. 5c). In trench-57, only subunit 2Ab was present. This subunit represents a soil layer with dark brown color. The yellow-brown subunit 2BC was only present in trench-41 (Fig. 2). The MS, TOM and median grain size show similar vertical variations in the three sections (Fig. 3). The MS has small variation at around 1.2×10^{-7} m^3/kg, and the TOM decreases slightly to 1.3 wt% (Fig. 3). The median grain size steadily increases from 100 to 200 μm

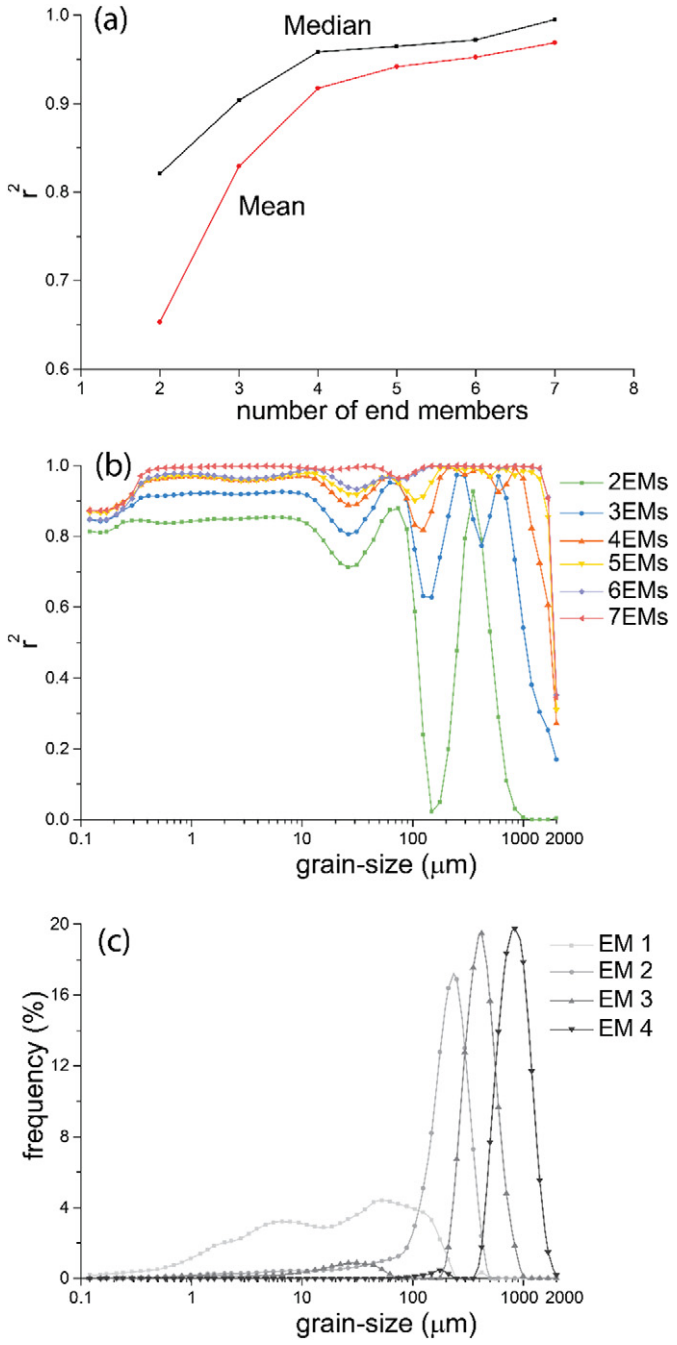

Fig. 4. The end-member modelling results. (a) The median and mean r^2 across all grain size classes as a function of the number of end members. A four-end-member model is sufficient to explain >95% of the total variance. (b) r^2 for each size class for end-member models with two to seven end members. (c) The end members according to the four-end-member model.

(Fig. 3). This is also reflected in the end-member modelling results, where the EM2 proportion increases upwards and accounts for >75%, at the expense of a decreasing EM1 (Fig. 3). EM3 occurs in very low abundances near the top of the unit, whereas EM4 is absent throughout unit 2.

4.2.5. Unit 1 (1C/1BC-1Ab)

Unit 1 differs from unit 2 by its coarse-grained texture and brownish yellow color (Fig. 5c). In trench-41, subunits 1C, 1BC and 1Ab were distinguished (Fig. 2a). At the eastern part of the levee, unit 1 overlies the older units 2–4 with an erosional contact related to reactivation of the Maas channel (Fig. 2a). In trench-57 only 1BC and 1Ab were exposed (Fig. 2b). Subunits 1BC/C consist of yellow-brown, silty to fine and coarse sand. The sediments in subunit 1Ab have a darker brown color and are coarser than underlying sediments. There are no clear laminae observed in this subunit and the depositional profile shows a homogenous structure.

From subunit 1BC to subunit 1Ab in sections A and C, the MS increases slightly from 1.1 to 2.2 × 10^{-7} m^3/kg (Fig. 3), and the TOM record generally shows first a decreasing trend in subunit 1BC, but subsequently an increasing trend in the soil layer corresponding with subunit 1Ab (Fig. 3). The TOM increase is most pronounced in section C (Fig. 3). The median grain size shows little variation (with averages of 200 μm) in sections A and C, but decreases from 200 to 140 μm in section B. Interestingly, all three sections show a similar trend in their cumulative EM graphs: a simultaneous increase of EM3 and EM1 at the expense of a EM2 decrease in subunit 1Ab (Fig. 6). This is different in the underlying units, in which the proportions of fine end members increase (decrease) as the coarse end members decrease (increase) (Fig. 6).

4.2.6. Unit 1/2 (½ BC, ½ Ab and ¾ Ab)

Unit 1/2 was discovered in the later stage of the archeological investigations and was not sampled. This unit is only present at the flanks of the levee (Fig. 2). The deposits have a similar texture as those of unit 1 and are coarser than the overlying OE sediments. Based on color and texture, three subunits were defined, ½ BC, ½ Ab and ¾ Ab. In the east, these sediments dip toward the Meuse channel (Fig. 2) and sharply overlie the older units 3 and 4 with an erosional contact (Fig. 2b). In trench-41, the ½ BC and ½ Ab subunits were present at the northeastern part of the levee, and ½ Ab and ¾ Ab were found at the southwestern part.

4.2.7. Units OE and JOD

The OE unit covers the subunits ½ BC, ½ Ab and ¾ Ab at the eastern flank (OE and JOD are abreviations for the Dutch words "oeverafzettingen" and "jong overstromingsdek", respectively). At the western part of trench-57, the OE unit directly overlies the subunit 1Ab. The OE unit was exposed in sections B and C (Fig. 3). The overlying JOD unit is subdivided into two parts: an upper plough sublayer (produced by modern farming) with darker color and an underlying previous plough sublayer with less organic matter and lighter color (Fig. 5d).

In the two units, the MS varies at 2.0 × 10^{-7} m^3/kg with a slightly increasing trend to ~3 × 10^{-7} m^3/kg toward the top of unit JOD. In section C, the TOM rapidly decreases from 4.5 to 1 wt% in OE and then increases to 1.5 wt% in the lower JOD sublayer, and in section B the TOM gently decreases from 2.7 to 1.5 wt% (Fig. 3). In the lower to middle intervals of OE (below the depth of 80 cm in section C and 90 cm in section B), the median grain size shows a decreasing trend, and the proportions of EM1 continue to increase whereas the proportion of EM3 decreases slightly. This feature is different from that in subunit 1Ab. Above the depth of 80 cm in section C and 90 cm in section B, the median grain size increases to ~240 μm in the JOD unit (Fig. 3). In line with this result, the proportion of EM1 decreases to 10% and the proportion of EM3 increases to 50% in JOD unit (Fig. 3). The proportion of EM1 in unit OE from section B is about two times higher than in section C. In the JOD unit, the proportions of EM1-EM3 reach similar values, but the coarsest EM4 also appears occasionally (Fig. 3).

4.3. Chrono-stratigraphic framework and age-model

Tebbens et al. (1999) obtained samples from the base of the OAC-1 paleochannel that were ^{14}C dated at 9170 ± 200 (calibrated median age: 10,369 BP; calibrated with IntCal 13 curve (Reimer et al., 2013)), which gives a minimum age of the OAC-1 channel abandonment. A ^{14}C date from the 4Ab subunit at the investigated levee (close to transect 2, Fig. 1C) produced an age of 8930 ± 40 (calibrated median age: 10,046 BP). Zuidhoff and Huizer (2015) reported an OSL age (9900 ±

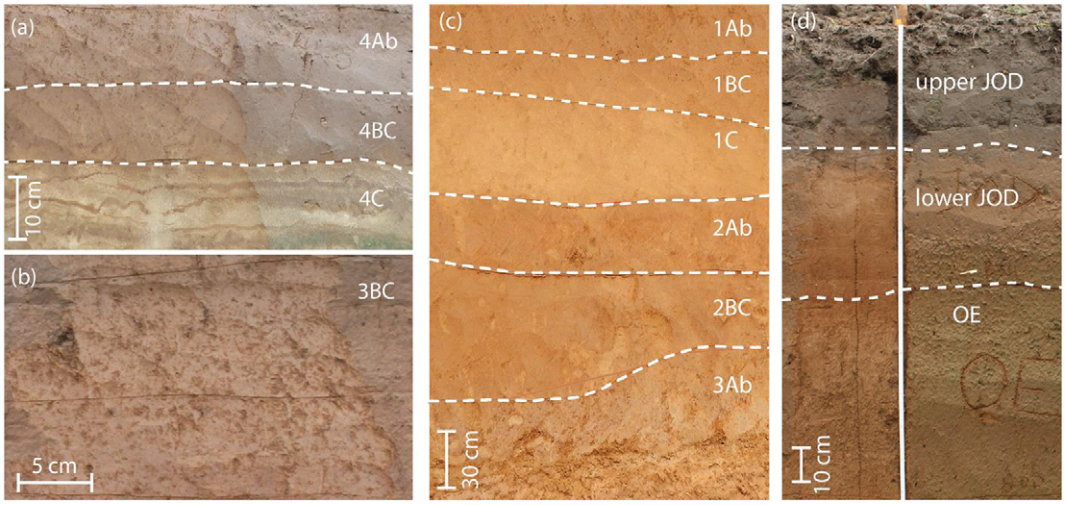

Fig. 5. Photographs of each (sub)unit of the Ooijen levee deposits. Dashed lines in each panel represent (sub)unit boundaries. (a) Unit 4 consists of sand at the base and shows a fining-upward trend in the grain size composition. Subunit 4C features horizontally bedded sand with some clay-iron illuviation laminae and 4Ab is a developed soil layer with brownish color. (b) Subunit 3BC has a brownish color and densely distributed burrows. (c) Unit 2 and overlying unit 1. Composition of subunit 2BC is coarser than the underlying 3Ab subunit. Subunit 1C has yellow-brown color and is coarser than the underlying 2Ab. Soil formation in 2Ab is less pronounced than in 3Ab. (d) Units OE and JOD exposed in the west part of trench-57. A clear boundary exists within JOD between the lower layer (previous plough sublayer) and the upper layer (plough sublayer).

900) for the point-bar deposits obtained from 1.9 m beneath the present-day surface (between transects 3 and 4, Fig. 1C). During this time the Meuse channel flowed at the present levee location. Considering the uncertainty, the time interval of the two ^{14}C ages (both calibrated ages fall into the middle Mesolithic) agrees with the OSL age and further constrains the minimum ages of subunits 4C and 4BC that formed during the early/middle Mesolithic.

In subunit 4Ab, the archeological findings of land use and habitation (fireplaces, flint processing sites and processed tools) feature early-middle Mesolithic characteristics (Fig. 7a). This is evidenced by a ^{14}C date (8930 ± 40, Table 1) at the base of 4Ab, which indicate an age for this subunit of ca. 10 ka cal BP. The estimated sedimentation rate is 9 cm/kyr for subunit 4Ab (Fig. 8).

At the transition of subunits 4Ab to 3BC, hearths and stone processing sites were found. The allochthonous materials, such as Wommersom quartzite and Obourg flint belong to the Sauveterrien cultural period (8.5–6.5 ka BP). Subunit 3BC showed a high intensity of land use and stone and flint processing, and a large number of artefacts (25,300 pieces of flints) that were dated in the late Mesolithic (8.4–6.9 ka BP) (Fig. 7b). Two ^{14}C dates provide a solid age for this period (Table 1). The sedimentation rate for 3BC is 17 cm/kyr. At the transition of subunit 3BC to 3Ab, late Mesolithic (8.4–6.9 ka BP) artefact assemblages were found (Fig. 7c), including flint processing sites and the first presence of potteries. Therefore, we conclude that subunit 3BC formed during the interval of 8.4–6.9 ka BP (Fig. 8). In the lower part of subunit 3Ab, potteries with Bischheim/Swifterbant and LBK (Linear Pottery Culture, 7.5–6.5 ka BP) cultural characteristics (Fig. 7d) were found. Hence, the lower 3Ab sediments may have formed at the transition to early Neolithic. In the surface of 3Ab, late Neolithic potteries, flints and natural stones were found (Fig. 7e). Therefore, the middle to top part of the subunit 3Ab was formed during the middle-late Neolithic, and two ^{14}C dates provide ages (Table 1) in agreement with a middle Neolithic period. Hence, subunit 3Ab was formed during the Neolithic (6.9–3.9 ka BP) and its sedimentation rate is about 9 cm/kyr (Fig. 8).

In the highest part of subunit 1Ab on the studied levee, Iron Age potteries and Middle Age artefacts were found. These two periods were separated on the flanks of the levee, in which the Iron Age findings were found in subunit 1Ab (Fig. 7f) while early Middle Ages findings were embedded within OE deposits. This indicates that subunits 1BC-1Ab have formed in the Iron Age and that the OE sequence as formed during the early Middle Ages (Dark Ages). Based on that, we calculate the sedimentation rates during the Iron Age and Middle Ages to be 45 cm/kyr and 21 cm/kyr, respectively. Therefore, subunit JOD was formed during the late Middle Ages as it overlies the Middle Ages pottery, and this is corroborated by an OSL date at the base of JOD. The sedimentation rate in JOD reached the largest level, 86 cm/kyr. Unit 1/2 was buried under the OE subunit and overlies subunit 1Ab. Therefore, unit 1/2 was likely formed during the time period between the Iron Age and early Middle Ages (possibly in the Roman Period). Constrained by the youngest findings (late Neolithic) in subunit 3Ab and the oldest findings (early-middle Iron Age) in subunit 1BC, it is reasonable to infer that subunit 2Ab was deposited during the Bronze Age. However, during the archeological investigation, little archeological finds were found that could provide solid evidence for a Bronze Age habitation on the levee. We obtained the sedimentation rate of 15 cm/kyr for Bronze Age.

Based on the above derived chronostratigraphic information, the age-depth model for each levee section is constructed (Fig. 8). In section A, the Roman Period and Middle Ages deposits are absent (Fig. 8). In section C and B, only the Roman Period deposits are absent (Fig. 8). To reflect the temporal variation of the paleofloods for each cultural period, the ages were linearly interpolated within each cultural period according to the upper and lower age boundaries. In Section 5.3 we discuss the rationality of this method.

4.4. Flood energy reconstruction based on decomposed levee grain size records

The distinctly different grain size distribution of EM1 in comparison to EM2-EM4 indicates that the fine-grained EM1 represents a different transport process than EM2-EM4. In addition, the consistent presence of EM1 in the four, five, six and seven end-member models imply that EM1 cannot be decomposed and represents a single transport process. In this levee context, we interpret the finest EM1 as suspended sediment load and coarse EM2-EM4 as bedload (a very similar mixing model has also been observed in Rhine fluvial sediments (Erkens et al., 2013)). The suspended load (EM1) and bedload (EM2-EM4) represent different hydrological/sedimentary transport processes. By constructing an index consisting of only the bedload end members, we are able to derive a proxy for flood energy variation, independent of the contribution of the suspended load.

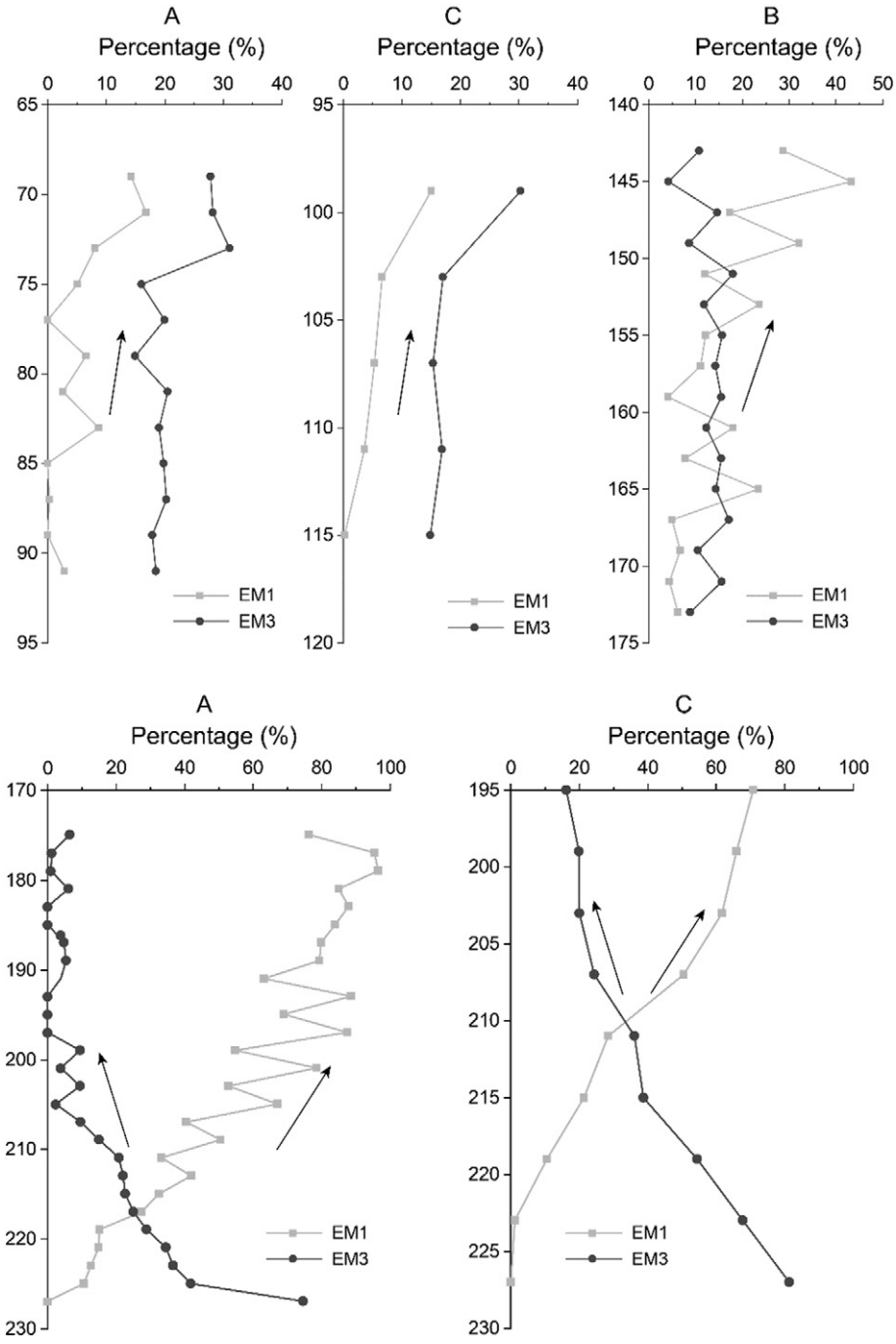

Fig. 6. The proportions of EM1 and EM3 in the four-end-member model in three sections from subunit 1Ab (upper panel) and 4BC-4Ab (lower panel). The variations of the two end members show that EM1 (suspended load) and EM3 (intermediate bedload component) increase simultaneously in subunit 1Ab, while in unit 4 they have opposite changes.

Our levee sediments based Flood Energy Index (LFEI) is based on the ratio of the coarsest bedload end members, EM3+EM4, over the total sum of the bedload end members EM2-EM4:

$$LFEI = (EM3 + EM4)/(EM2 + EM3 + EM4) \quad (1)$$

The LFEI records and the chronological information for the three sections are plotted against depth in Fig. 8. Because subunit 4C represents the top of point-bar deposits underlying the levee sediments (see Section 5.1) and no archeological artefacts were found in subunit 4BC, this study only focuses on the paleofloods since the middle Mesolithic (subunit 4Ab, from ca. 10,590 a BP). The raw LFEI variation for each section was processed by using a locally weighted polynomial smoothing function (LOESS) to prevent placing undue emphasis on single data points (Fig. 8). The temporal variation of the LFEI is shown for each levee section in Fig. 9.

5. Discussion

5.1. Longitudinal differential levee sedimentation

Unit 4 consists of coarse sand and sand-clay deposits, which in this fluvial context should be interpreted as channel or point-bar deposits and overlying floodplain deposits. Subunit 4C constitutes the top of point-bar deposits that formed during channel migration. Evidence are the coarse grain size characteristics (Fig. 3) and the embedded

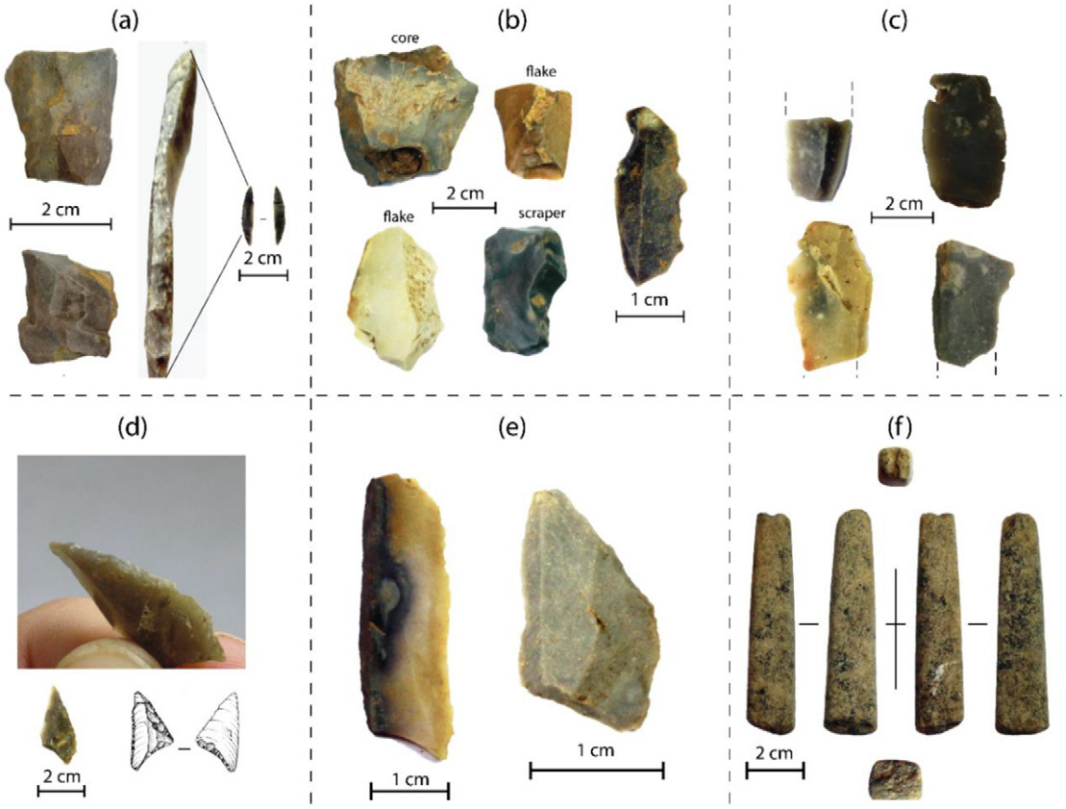

Fig. 7. Selected artefacts from the archeological investigations (Ellenkamp et al., 2018) on the levee from different cultural periods. (a) Lanceolate microlith-point with totally retouched side-edge from subunit 4Ab. (b) Late Mesolithic denticulate blade from 3BC subunit. The four on the left are a core, a flake and a scraper made from flint. The one on the right is a flint tool. (c) Upper-left is the lithic flake found at the 3BC-3Ab interface (late Mesolithic), and its distal end was made from glassy flint. The other three are flints used for lithic manufacturing processes. (d) Trapezoidal point with retouched long edge and base-point from 3Ab subunit with Neolithic feature. (e) Left is a micro-blade made from coastal-flint pebble, right one is a trapeze with broken top-end (impact-fracture) from the upper part of 3Ab. (f) Iron Age wetstones or fragments of stone pendant with a quadrangular cross section discovered in subunit 1C. The tools are made of fine-grained stones and were processed to smoothen and flatten their surface.

shell fragments, indicating a riverine environment. The fine-grained deposits from subunit 4BC to unit JOD formed after the channel had migrated to its present position. This means that the paleohydrological information, derived from the sedimentary analyses and archeological investigations, reflects the overbank flooding regime with vertical aggradation that was not influenced by lateral river migration.

Table 1
Chrono-stratigraphical framework of the Ooijen site (after Ellenkamp et al., 2018).

Stratigraphy	Archeological period	^{14}C/***OSL*** dating	Typological dating of flint	Typological dating of pottery
JOD	Post-Middle Ages	***790 ± 70***		
OE	Middle Ages			
¾ Ab, ½ BC, ½ Ab	Roman Period			
1BC-1Ab	Iron Age			Iron Age pottery
2Ab	Bronze Age			
Mid-upper 3Ab	Neolithic	4900 ± 40 (5631)[b] 4440 ± 40 (5050)[b]	Mid-late Neolithic artefacts	Mid-late Neolithic pottery
Lower 3Ab	Mesolithic-early Neolithic		Flint assembly with Mesolithic characteristics	Bischheim/Swifterbant and LBK pottery
3BC-3Ab			Artefacts with late Mesolithic characteristics	First appearance of pottery
3BC	Late Mesolithic	6660 ± 40 (7534)[b] 6450 ± 40 (7367)[b]	Many artefacts with dates between middle and late Mesolithic	
4Ab-3BC			many artefacts with dates between middle and late Mesolithic, including Sauveterrien period	
4Ab	Early-middle Mesolithic	8930 ± 40 (10046)[b]	Many processed artefacts dated to early-middle Mesolithic	
4BC	Early-middle Mesolithic[a]			
4C				

Age in JOD is OSL dated (Ruijters et al., 2017) and is given in bold italic form, the ages in underlying units are ^{14}C dated (Ellenkamp et al., 2018). The numbers in parentheses are calibrated median ages. The calibration is performed with IntCal 13 curve (Reimer et al., 2013).

[a] The deposition period is inferred based on the stratigraphic relationships and paleo-channel study (see Section 4.3).

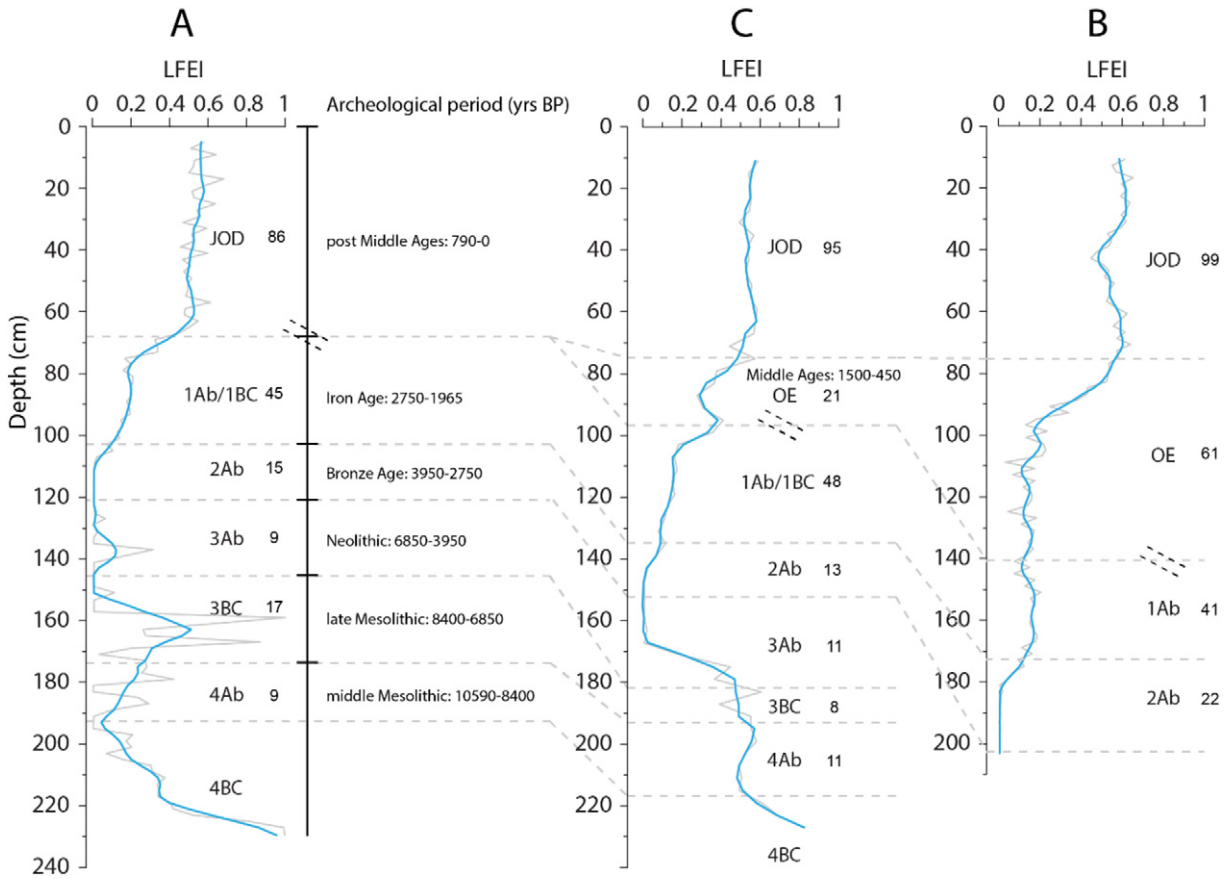

Fig. 8. The levee-based flood energy index (LFEI) and chrono-stratigraphic correlations. The grey curves represent all data points. The blue curves are smoothed LFEI records by using a locally weighted polynomial smoothing function (LOESS) to prevent undue emphasis being placed on single data points. The horizontal dash lines indicate the boundary of each cultural period in each section. The diagonal dash lines indicate the sedimentary hiatus. The numbers along the curve are calculated sedimentation rate (cm/kyr) in each period. In section A, the Roman Period and Middle Ages deposits are absent. In section C and B, only the Roman Period deposits are absent.

The DEM analyses showed that the studied location is situated on a levee. The stratigraphic build-up and lithological composition show that the subunits 4BC to JOD are also deposited in a levee environment. For example, the convex lower units 3 and 4 represent a small levee in an early stage of deposition.

The accumulation process of the NW part of the levee is different from that of the SE part. Previous archeological investigations on the SE part of the levee (site 4 in Fig. 1C) have shown near-surface Neolithic pottery (Heunks, 2000). Hence it was concluded that the SE part of the levee was stable (almost no deposition) in the past ~7 ka. This is in strong contrast with the NW part of the levee, in which sediments were deposited with archeological remnants from the Mesolithic to the Middle Ages or Present. This indicates a different sedimentary and geomorphological evolution for the two parts of the levee. Two reasons are proposed to explain this. First, the northern part, where trench-57 and trench-41 are located, is situated on the more downstream inner bank of the channel bend (Fig. 1C). Small northeastward bend migration will have resulted in space for deposition on the inner bank. Conversely, the part of the levee at site 4 is located next to a straight channel that had nearly no lateral migration (Fig. 1C). Therefore, limited space has been produced for deposition at site 4. The second explanation is based on the slope of the crest of the levee during the early Holocene. Based on DEM information, the present average elevation at the NW part of the levee (trench-57) is ~14.6 m, which is ~90 cm lower than the SE part (Fig. 1D). A lower elevation at the NW part of the levee will have favored more sedimentation during flooding.

Unlike a commonly seen continuous sedimentation in floodplain settings, the Ooijen levee shows that sedimentation rates can be variable along a levee at the channel bend scale because of different deposition processes. This agrees with previous research in the region in which it was concluded that sedimentation and morphology varies between river bends and even within a single bend (Ruijters et al., 2017). Therefore, morphological pre-investigations should be performed for locating the best spot (continuous sedimentation) on a levee for flooding reconstructions.

5.2. The influence of flooding phases and human activity on levee sedimentation

The paleoflood reconstruction is based on grain size analysis of sediment units, soil characteristics and archeological finds that enable chronological control. During floods and flooding phases the sedimentation was more prominent, while soil formation and human activity were more important during low flooding conditions. However, it is emphasized that sedimentation, soil formation and occupation are not mutually exclusive on a levee setting. The increasing degree of soil formation (Ab layers) with depth (Fig. 5a–c), and the absence of parental materials (C horizons) indicate that the deposited sediments were transformed into soils immediately after sedimentation. Thus, soil formation and sedimentation took place concurrently on the levee. One should also bear in mind that other factors, for instance, the vertical growth of the levee, the change of sediment source and composition, and channel migration may complicate the interpretation of flooding variations. For example, the aggradation of sediments on the levee elevated its surface and this increases the threshold of bankfull discharge. In addition, human activity in the Meuse catchment since the Neolithic

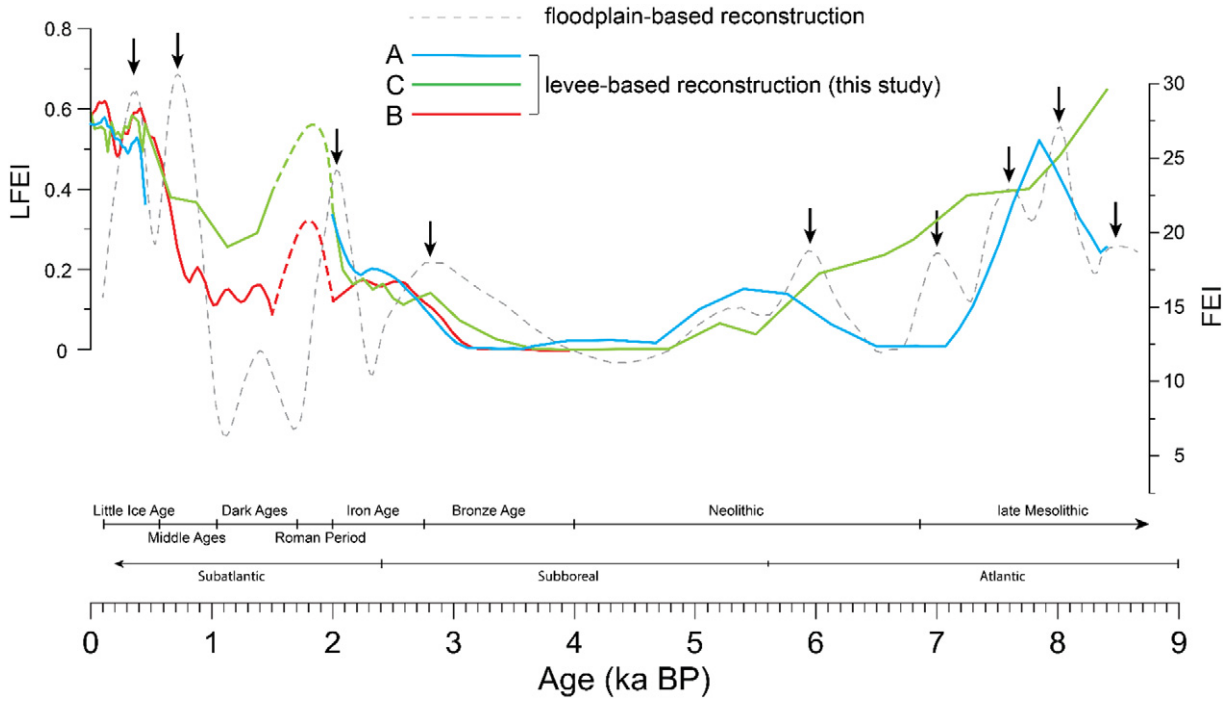

Fig. 9. Holocene Lower Meuse paleoflood reconstructions based on floodplain sediments (FEI, grey dashed line) (Peng et al., 2019) and levee sediments (LFEI, colored lines, this study). The two independent reconstructions show a gradually weakened flooding regime during the Mesolithic followed by a low sedimentation rate and flooding activity during the Neolithic and Bronze Age. Instability of the fluvial behavior since the Iron Age is evidenced by a high sedimentation rate and more severe flooding. This trend is interrupted by the lower flooding phase in the early Middle Ages (Dark Ages). Colored dashed lines are inferred from the field observations (see Section 5.2.3).

has altered the sediment source and therefore the grain size characteristics of the sediment input to the fluvial system. Model simulations and field sediment investigations have shown that deforestation and farming from the mid-Holocene onwards in the Meuse catchment led to severe soil erosion and increased floodplain sedimentation, and to increased discharges (De Moor et al., 2008; Ward et al., 2008; Bos and Zuidhoff, 2015). A higher sediment load caused by increased anthropogenic activity will be reflected by higher sedimentation rates on the levee. Our LFEI index, however, reflects variations in flooding energy, which are the combined result of climate change (precipitation) and land-use change. Deforestation and agriculture activities resulted in increased runoff caused by decreased interception and evapotranspiration and less infiltration.

5.2.1. Decreasing flooding during the late Mesolithic

We interpret the 4BC as the transition from the point-bar environment to a levee setting, and this is shown by the gradually reduced grain size (Fig. 3). Gradually reduced river flooding since the middle Mesolithic can be inferred from the fine-grained subunit 4Ab-3BC deposits (Fig. 3), and from the high proportion of fine EM1 and low proportion of coarse EM2-EM4. The low flooding regime in the later stage of the Mesolithic partly accounts for the highly developed soil layers (4Ab-3BC) that are evidenced by high TOM and MS. The 3BC sediments show similarities with the underlying 4Ab subunit in section A with well-developed soil formation and fine sediments (Fig. 5a, b) implying the two subunits likely formed in the same flooding regime. The densely distributed burrows in 3BC are indicative for strong bioturbation. Bioturbation is unlikely to happen during a high flooding regime. A regime of lower river flooding activity favored prehistoric humans' occupation on the levee in the middle Mesolithic. The ^{14}C results and archeological findings (Table 1) from the two subunits indicate they formed during the middle Mesolithic (4Ab) and the late Mesolithic (3BC). The LFEI variations determined from section A decrease steadily through the late Mesolithic. This implies a reduced deposition of the coarsest bedload components, and thus lower flooding intensity. The low flooding conditions persisted through the late Mesolithic (subunit 3BC) until the start of the Neolithic (subunit 3Ab). During the late Mesolithic, anthropogenic activities increased, as indicated by the wide distribution of the different artefact types on the levee (Table 1, Fig. 7b–d), including homogenous flint concentrations, processed stones (these indicate that the research area had been a site for flint processing) and fireplaces. The archeological investigations concluded that the levee has been occupied for a long time during the Mesolithic period (Ellenkamp et al., 2018), but the human impact on the landscape was still limited (Bos and Zuidhoff, 2015; Peng et al., 2019) and unlikely to have resulted in an apparent change in the sediment source and composition. The low sedimentation rate (Fig. 8) supports this interpretation. The levee, directly seated on a point-bar deposit (subunit 4C), was at a juvenile stage at that time. These observations agree with the reduced LFEI, representing subdued flooding and decreased discharge on a millennial-scale. The top of subunit 3BC has a relatively flat surface, which differs from the upper surface of underlying unit 4 (Fig. 2). This may be a result of long-term human activity that has flattened the ground surface.

5.2.2. Low to moderate fluvial activity during the Neolithic and Bronze Age

The Neolithic and Bronze Age sedimentary records show a coarsening-upwards trend, with a decrease of the proportion of fine EM1 (3Ab and 2Ab subunits in Fig. 3), indicating that the Lower Meuse changed from a low flooding regime in the early Neolithic into a moderate flooding regime during the late Neolithic and Bronze Age. In addition to the sedimentary observations, the magnitudes of the LFEI index in sections A and C also evidence a moderate flooding phase in the middle Neolithic and in the late Bronze Age, in between a low flooding intensity from the late Neolithic to the middle Bronze Age (Fig. 9). Middle to late Neolithic potteries and flints were found at the top of subunit 3Ab (Ellenkamp et al., 2018). The artefacts have a higher distribution density than the lower Mesolithic ones. This is mainly caused by a change in human behavior using the levee more intensively during the Neolithic than during the Mesolithic (Ruijters et al., 2017). Furthermore, the charcoal spots that were observed in subunit

3Ab, could be caused by human-induced fire events. These findings indicate a stable environment and human settlement during the Neolithic.

In the Well-Aijen floodplain area, which is located ~9 km NW of Ooijen (Fig. 1B), an increase of crop plants species (i.e., *Cerealia*, *Plantago lanceolata* and *Anthoceros punctatus*) was identified at the start of the Neolithic (Bos and Zuidhoff, 2015), indicating the increase of agricultural activities in the surrounding landscape (Bos and Zuidhoff, 2015). The small increase of the LFEI flooding index during the middle Neolithic (Fig. 9) may thus be related to increased runoff caused by farming and deforestation.

Very limited Bronze Age artefacts have been discovered in subunit 2Ab, hinting at a reduction of human activity on the levee. The soil formation in subunit 2Ab is less pronounced compared to the soil subunits 3Ab and 4Ab (Fig. 5a–c). Bos and Zuidhoff (2015) reported that human activity was still present in the Well-Aijen area but less pronounced than in the early-middle Neolithic (Fig. 1B). In the Netherlands and other regions of northwestern Europe, a population decline and socio-economic collapse at the end of the Bronze Age have been suggested (Van Geel et al., 1996; Gerritsen, 2003; Armit et al., 2014). However, the causal relationship of the moderate flooding regime in the later stage of the Bronze Age and less human occupation on the levee is unclear, as this deterministic idea that population collapse at the end of the northwestern European Bronze Age was caused by rapid climate change in the Atlantic region is still under debate (i.e., Van Geel et al., 1996; Tipping et al., 2008; Armit et al., 2014).

5.2.3. High flooding and rapid sediment accumulation since the Iron Age

In the Iron Age, the direct evidence of gradually enhanced flooding is shown by the coarse median grain size of unit 1 and the increase of EM3 (bedload component) from subunit 1BC upwards, though the median grain size value decreases slightly in section B (Fig. 3). The archeological excavation revealed evidence of erosion by the Meuse of the eastern flank of the levee, where parts of units 2–4 were eroded during the Iron Age (Fig. 2). The gradual combined increase of LFEI and sedimentation rate at the start of the Iron Age suggests that both are mainly caused by increased flooding. During the Roman Period (unit 1/2), erosion occurred at the eastern flank (Fig. 2b) which implies a high-energy depositional environment. This unit has not been sampled. During the archeological investigations, the sediments in this unit appeared coarser than the overlying OE unit. Therefore, we infer a more dynamic fluvial condition in the Roman Period compared to the early Middle Ages (Dark Ages). In the early Middle Ages, a decrease of the median grain size, a continuous increase of the fine EM1 (suspended load) and a decrease of the EM2-EM3 proportions in the lower to middle part of the OE unit are observed (Figs. 3 and 8). Low values of LFEI (Fig. 9) indicates a phase of relatively low flood magnitudes. It should be noted that the overall flooding activity inferred from LFEI in this period was still higher than in earlier times (Mesolithic). Since the middle to late Middle Ages a coarsening-upward trend occurred and the bedload end members are dominant (Fig. 3, upper part of OE). Minor contributions of the coarsest end member EM4 (with a mode at 840 μm) likely reflect intensified flooding after the Middle Ages (Fig. 3). High floods since the Iron Age seem likely considering the elevated levee height, because floods with constant and/or decreased magnitude were unlikely to have caused erosion of unit 4 and a coarsening-upward sequence.

In the Iron Age deposits (subunit 1Ab), the increased proportion of the fine end member (EM1, representing suspended load) in the upper part of subunit 1Ab (Fig. 6) indicates a relatively low-energy sedimentary environment. At the same time, the increased proportion of EM3 (Fig. 6) points to high-energy hydrodynamic conditions. Another characteristic of this levee is that the convex slope is gradually decreasing since the deposition of unit 1 (Fig. 2). Both the end member variation and the gradually flattened levee surface can be explained by the re-opening of the paleochannel OAC-1. This paleochannel is ~1 m lower than its present surrounding area and extends to the SE where it connects to the Meuse channel (Fig. 1C). During peak discharge events, water flowed through the depression, which could serve as a chute channel to accommodate excess water and carry suspended sediments to the west flank of the levee. The proximity of the west flank (sections B and C) to paleochannel OAC-1 could have led to relatively long-term inundation because the two sections were located at the lower elevations since the Iron Age (Fig. 2b). Consequently, the fine sediments (EM1) settled after the initial deposition of coarse sediments (EM2 and EM3). This interpretation agrees with units 2–4 being thicker in section A than in section B; whereas the younger subunits 1Ab and OE in section B are thicker than in A and C. In addition, the higher proportion of EM1 in OE in section B compared to section C also supports this interpretation. An active flooding phase during the Iron Age seemingly disagrees with the archeological results, since Iron Age pottery was found in the top of 1Ab, indicating anthropogenic occupation and suggesting less flooding. We propose this is associated with the high elevation of unit 1 (Fig. 2). From the early Iron Age (subunit 1BC), higher peak discharges with coarse sediments could reach the levee. However, the elevated levee was only inundated temporarily, and humans could re-occupy the levee after floods. A recent modelling study (Johnston et al., 2019) supports our explanation. The simulations reveal that small levees are inundated from crest to distal areas as floodwaters spill out of the channel and flow down the levee. On a mature high levee, floodwaters flow around the levee perimeter and inundate the distal levee first, causing the highest deposition rate at the distal part because it is inundated longest with sediment-laden floodwater. This inundation behavior has also been described by Filgueira-Rivera et al. (2007) for the Columbia River (Canada), where less severe floods preferentially aggrade the distal levee areas, resulting in long periods of inundation and more rapid deposition of the distal levee.

In the Well-Aijen area (Fig. 1B), a paleoecological study (Bos and Zuidhoff, 2015) shows that the apparent increase of heather species (which favor nitrogen and phosphate-poor soils) in the Iron Age was the result of over-cultivation and grazing. In the Lomm and Boxmeer areas (Fig. 1A), evidence of increased floods during the Iron Age was also found (Zuidhoff and Bos, 2011a, 2011b). In the central part of the Netherlands, a shift to a wetter climate at the start of the Iron Age (~2800 BP) has been demonstrated based on vegetation reconstruction and lake-level changes (Van Geel et al., 1996; Engels et al., 2016; Van den Bos et al., 2018). In the Roman Period and the subsequent mid-late Middle Ages, the Lower Meuse catchment experienced large-scale deforestation, farming, channel regulation and population expansion, resulting in severe soil erosion, increased overbank sedimentation and increased runoff (Fig. 8; De Moor et al., 2008; Ward et al., 2009). These human factors, coupled with the wet and warm summers (Büntgen et al., 2011) during the late Holocene, together contributed to the increased flooding intensity and coarse sediment deposition. The erosion surface during the Iron Age (Fig. 2), and the significant increase of the sedimentation rate, indicate the human-induced changes dominate over the climate factor in the late Holocene.

5.3. Applicability of Ooijen levee sediments in paleoflood reconstruction

The focus of this study is to explore the potential of using levee deposits in paleoflood reconstruction, instead of studying the factors that determine levee formation and evolution. However, we are aware that levee development can also affect the relation of floods with deposition. For instance, changes in channel dimension and discharge, lateral channel migration, changes in sediment supply, changes in flood basin configuration (connection between channel and floodplain) and bed forms may all affect levee deposition (e.g., Törnqvist and Bridge, 2002; Adams et al., 2004; Pierik et al., 2017). Therefore, using sedimentary archives from levees for paleoflood studies is not straightforward because levee growth is conventionally regarded as a dynamic process, leading to a lower sediment preservation potential than floodplain and lacustrine sediments. For instance, in the Roer Valley Graben in the Lower Meuse catchment, the Holocene Meuse River shows highly sinuous channels

and active lateral migration; therefore, it is impractical to conduct paleoflood reconstruction from such levee sediments because the levees are young and susceptible to channel migration. In this context, levee deposition is not the first choice in a paleohydrological study if other more suitable fluvial archives are available. However, the Ooijen levee demonstrates advantages related to the well-preserved stratigraphy, limited Holocene channel migration and good archeological dating control. In addition, gradual channel downcutting during the Holocene is unlikely to have influenced the grain size record. The elevation of the top of the point-bar and channel sands below the levee does not show an incisional trend toward the present-day Meuse River. Downcutting behavior of the Lower Meuse was more notable during the climate transition from the Late Glacial to the Holocene (Kasse et al., 1995; Tebbens et al., 1999). In addition, the relative subsidence of the Venlo Block (Van Balen et al., 2005) and gradually increased sediment input from the Meuse catchment in the middle to late Holocene (Ward et al., 2009) do not favor river incision. The archeological results were used to constrain the stratigraphic age in this study. The archeological finds of several cultural periods are in a vertically stacked sequence and mixing of artefacts from different periods in one unit was hardly observed (no palimpsest horizons). We are aware of the potential existence of erosive or non-depositional surfaces during levee formation. It is possible that decadal hiatuses are present. However, the stacked archeological findings (from early Mesolithic to the Middle Ages) clearly indicate that deposition was continuous on a centennial to millennial scale. Based on these considerations, aided with the archeological investigations and vegetation development studies, the Ooijen site is regarded to contain a reliable flooding record.

Peng et al. (2019) analyzed the Holocene paleoflooding history of the Lower Meuse in a floodplain setting at Well-Aijen (Fig. 1B). The flooding reconstruction results are shown in Fig. 9, alongside the LFEI flooding index record based on the end-member modelling results for the three levee sections at the Ooijen site presented in this study. Comparison of the two independent reconstructions from different settings shows that they agree quite well: both show a gradually weakened flooding regime since the late Mesolithic (Atlantic period) followed by a low sedimentation rate and flooding activity during the Neolithic and Bronze Age (Subboreal period) (Fig. 9). An increased dynamic fluvial behavior since the Bronze Age (Subatlantic period) is evidenced by a high sedimentation rate and more severe flooding (Fig. 9). This trend was interrupted by short lower flooding phases in the Iron Age and early Middle Ages (Dark Ages). The comparison of the two reconstructions indicates that well-preserved levee deposits can also be used to determine the history of paleoflooding regimes.

6. Conclusion

We applied grain size analyses, end-member modelling, magnetic susceptibility and thermogravimetric analyses to a sedimentary record on a levee to infer flooding intensities, and combined it with archeological evidence, to arrive at a Holocene paleoflooding history of the Lower Meuse in the Netherlands. The flooding intensity changes are a combined result of human land-use change (deforestation and agriculture) and climatic changes (precipitation) and the land-use change also caused variation in sedimentation rates, which indicates that the human-induced changes dominate over the climate since the Iron Age. Starting from the middle Mesolithic, the results reveal a gradually decreasing and low flooding regime in the Mesolithic, during which the young levee was low. In this period, humans began to occupy the levee but the anthropogenic influence on the landscape in the Lower Meuse valley was still low. The appearance of humans on the levee agrees with the inferred reduced flooding intensity. Subsequently, the Neolithic and Bronze Age periods experienced a low, but gradually increasing flooding regime. The Iron Age witnessed the start of a period of enhanced flooding with the deposition of coarser sediments. Intense flooding conditions lasted through the Roman Period until the early Middle Ages (Dark Ages), during which the Lower Meuse experienced a phase of weakened flooding intensity. From the middle to the late Middle Ages, the flooding conditions intensified again. We propose that the coarsening-upward trend and high accumulation rates since the Iron Age resulted from increased flooding and high sediment supply caused by human interference in the Meuse catchment.

Former investigations revealed that the SE part of the levee had little sedimentation in the last seven thousand years, whereas more recent archeological investigations showed that the NW part of the levee has preserved a continuous sedimentary record from the Mesolithic onwards. This different depositional history between two sites on the same levee can be attributed to the channel evolution and elevation difference. This indicates that morphological pre-investigations are critical for determining the optimal location for stratigraphic and sedimentological paleoflood investigations in a levee setting.

The general findings of this study agree well with a paleoflood reconstruction for the Lower Meuse valley ~9 km downstream, which was based on the grain size characteristics of fine-grained, suspended-load dominated lake and floodplain sediments. This implies that well-preserved levee sediments, along stable channel courses, can be a suitable candidate for paleohydrological studies.

Declaration of competing interest

The author(s) declared no potential conflicts of interest with respect to the research, authorship, and/or publication of this article.

Acknowledgments

We appreciate the assistance of many archaeologists who were involved in archeological investigations in the Ooijen-Wanssum area in the Netherlands. We would like to thank Martine Hagen and Unze van Buuren (Vrije Universiteit Amsterdam) for their assistance in laboratory analyses, P. Kubistal (BAAC) for identification of archeological artefacts. This research was supported by a China Scholarship Council fellowship to F. Peng.

References

Adams, P.N., Slingerland, R.L., Smith, N.D., 2004. Variations in natural levee morphology in anastomosed channel flood plain complexes. Geomorphology 61 (1), 127–142. https://doi.org/10.1016/j.geomorph.2003.10.005.

Allen, J.R.L., 1965. A review of the origin and characteristics of recent alluvial sediments. Sedimentology 5 (2), 89–191. https://doi.org/10.1111/j.1365-3091.1965.tb01561.x.

An, Z., Kutzbach, J.E., Prell, W.L., Porter, S.C., 2001. Evolution of Asian monsoons and phased uplift of the Himalaya–Tibetan plateau since Late Miocene times. Nature 411, 62. https://doi.org/10.1038/35075035.

Ao, H., Deng, C., Dekkers, M.J., Liu, Q., 2010. Magnetic mineral dissolution in Pleistocene fluvio-lacustrine sediments, Nihewan Basin (North China). Earth Planet. Sci. Lett. 292 (1), 191–200. https://doi.org/10.1016/j.epsl.2010.01.035.

Armit, I., Swindles, G.T., Becker, K., Plunkett, G., Blaauw, M., 2014. Rapid climate change did not cause population collapse at the end of the European Bronze Age. Proc. Natl. Acad. Sci. 111 (48), 17045–17049. https://doi.org/10.1073/pnas.1408028111.

Benito, G., Thorndycraft, V.R., Rico, M., Sánchez-Moya, Y., Sopeña, A., 2008. Palaeoflood and floodplain records from Spain: evidence for long-term climate variability and environmental changes. Geomorphology 101 (1), 68–77. https://doi.org/10.1016/j.geomorph.2008.05.020.

Bos, J.A.A., Zuidhoff, F.S., 2015. De restgeul van Well-Aijen. Een reconstructie van de vegetatieontwikkeling van het Noord-Limburgse Meusedal gedurende het Holoceen (Mesolithicum-Vroeg Romeinse tijd). ADC-rapport 3599, ADC Archeo Projecten, the Netherlands.

Boyle, J., 2004. A comparison of two methods for estimating the organic matter content of sediments. J. Paleolimnol. 31 (1), 125–127. https://doi.org/10.1023/B:JOPL.0000013354.67645.df.

Brierley, G.J., Ferguson, R.J., Woolfe, K.J., 1997. What is a fluvial levee? Sediment. Geol. 114 (1), 1–9. https://doi.org/10.1016/S0037-0738(97)00114-0.

Brook, G.A., Srivastava, P., Marais, E., 2006. Characteristics and OSL minimum ages of relict fluvial deposits near Sossus Vlei, Tsauchab River, Namibia, and a regional climate record for the last 30 ka. J. Quat. Sci. 21 (4), 347–362. https://doi.org/10.1002/jqs.977.

Büntgen, U., Tegel, W., Nicolussi, K., McCormick, M., Frank, D., Trouet, V., Kaplan, J.O., Herzig, F., Heussner, K.-U., Wanner, H., Luterbacher, J., Esper, J., 2011. 2500 years of European climate variability and human susceptibility. Science (New York, N.Y.) 331 (6017), 578–582. https://doi.org/10.1126/science.1197175.

Cunningham, A.C., Wallinga, J., 2012. Realizing the potential of fluvial archives using robust OSL chronologies. Quat. Geochronol. 12, 98–106. https://doi.org/10.1016/j.quageo.2012.05.007.

De Moor, J.J.W., Kasse, C., van Balen, R., Vandenberghe, J., Wallinga, J., 2008. Human and climate impact on catchment development during the Holocene-Geul River, the Netherlands. Geomorphology 98 (3), 316–339. https://doi.org/10.1016/j.geomorph.2006.12.033.

Duller, G.A.T., 2004. Luminescence dating of quaternary sediments: recent advances. J. Quat. Sci. 19 (2), 183–192. https://doi.org/10.1002/jqs.809.

Ellenkamp, G.R., Kubistal, P., Ruijters, M.H.P.M., Bloo, S.B.C., Ball, E.A.G., 2018. Vuursteen in lagen. Vindplaats 10 in projectgebied Ooijen-Wanssum, gemeente Horst aan de Maas. Archeologisch vooronderzoek: een waarderend veldonderzoek, the Netherlands.

Engels, S., Bakker, M.A.J., Bohncke, S.J.P., Cerli, C., Hoek, W.Z., Jansen, B., Peters, T., Renssen, H., Sachse, D., van Aken, J.M., van den Bos, V., van Geel, B., van Oostrom, R., Winkels, T., Wolma, M., 2016. Centennial-scale lake-level lowstand at Lake Uddelermeer (the Netherlands) indicates changes in moisture source region prior to the 2.8-kyr event. The Holocene 26 (7), 1075–1091. https://doi.org/10.1177/0959683616632890.

Erkens, G., Toonen, W.H.J., Cohen, K.M., Prins, M.A., 2013. Unravelling mixed sediment signals in the floodplains of the Rhine catchment using end member modelling of grain size distributions, 10th International Conference on Fluvial Sedimentology. University of Leeds 109–110.

Farrell, K.M., 1987. Sedimentology and Facies Architecture of Overbank Deposits of the Mississippi River, False River Region, Louisiana. In: Ethridge, F.G., Flores, R.M., Harvey, M.D. (Eds.), Recent Developments in Fluvial Sedimentology (SEPM Society for Sedimentary Geology).

Ferguson, R.J., Brierley, G.J., 2002. Levee morphology and sedimentology along the lower Tuross River, south-eastern Australia. Sedimentology 46 (4), 627–648. https://doi.org/10.1046/j.1365-3091.1999.00235.x.

Filgueira-Rivera, M., Smith, N.D., Slingerland, R.L., 2007. Controls on natural levée development in the Columbia River, British Columbia, Canada. Sedimentology 54 (4), 905–919. https://doi.org/10.1111/j.1365-3091.2007.00865.x.

Fisk, H.N., 1944. Geological Investigation of the Alluvial Valley of the Lower Mississippi River (Vicksburg).

Fisk, H.N., 1947. Fine-grained alluvial deposits and their effects on Mississippi River activity. Waterways Experiment Station, Vicksburg (Miss.).

Fuchs, M., Owen, L.A., 2008. Luminescence dating of glacial and associated sediments: review, recommendations and future directions. Boreas 37 (4), 636–659. https://doi.org/10.1111/j.1502-3885.2008.00052.x.

Gerritsen, F., 2003. Local Identities: Landscape and Community in the Late Prehistoric Meuse-Demer-Scheldt Region (Amsterdam Archaeological Studies, 9). Amsterdam University Press.

Heiri, O., Lotter, A.F., Lemcke, G., 2001. Loss on ignition as a method for estimating organic and carbonate content in sediments: reproducibility and comparability of results. J. Paleolimnol. 25 (1), 101–110. https://doi.org/10.1023/A:1008119611481.

Herb, C., Zhang, W., Koutsodendris, A., Appel, E., Fang, X., Pross, J., 2013. Environmental implications of the magnetic record in Pleistocene lacustrine sediments of the Qaidam Basin, NE Tibetan Plateau. Quaternary international 313, 218–229. https://doi.org/10.1016/j.quaint.2013.06.015.

Heunks, E., 2000. Project Zandmaas, deelgebied Ooijen, een Aanvullende Archeologische Inventarisatie (AAI). RAAP-rapport 498, Amsterdam.

Huisink, M., 1999. Lateglacial river sediment budgets in the Mass valley, The Netherlands. Earth Surface Processes and Landforms 24 (2), 93–109. https://doi.org/10.1002/(SICI)1096-9837(199902)24:2%3C93::AID-ESP940%3E3.0.CO;2-R.

Isarin, R.F.B., Rensink, E., Ellenkamp, G.R., Heunks, E., 2017. Of Meuse and Man: the geomorphogenetic and archaeological predictive maps of the Dutch Meuse valley. Neth. J. Geosci. 96 (2), 183–196. https://doi.org/10.1017/njg.2017.5.

Johnston, G.H., David, S.R., Edmonds, D.A., 2019. Connecting fluvial levee deposition to flood-basin hydrology. Journal of Geophysical Research: Earth Surface 0(ja). https://doi.org/10.1029/2019JF005014.

Kasse, C., Vandenberghe, J., Bohncke, S.J.P., B., F., Vandenberghe, J., 1995. Climatic change and fluvial dynamics of the Maas during the Late Weichselian and Early Holocene. In: Kasse, C., Bohncke, S.J.P., B, G. (Eds.), European River Activity and Climatic Change During the Lateglacial and Early Holocene. Paläoklimaforschung, pp. 123–150.

Knox, J.C., 2006. Floodplain sedimentation in the Upper Mississippi Valley: natural versus human accelerated. Geomorphology 79 (3), 286–310. https://doi.org/10.1016/j.geomorph.2006.06.031.

Kochel, R.C., Baker, V.R., 1982. Paleoflood hydrology. Science (New York, N.Y.) 215 (4531), 353. https://doi.org/10.1126/science.215.4531.353.

Konert, M., Vandenberghe, J.E.F., 1997. Comparison of laser grain size analysis with pipette and sieve analysis: a solution for the underestimation of the clay fraction. Sedimentology 44 (3), 523–535. https://doi.org/10.1046/j.1365-3091.1997.d01-38.x.

Lee, S.H., Lee, Y.I., Yoon, H.I., Yoo, K.-C., 2008. East Asian monsoon variation and climate changes in Jeju Island, Korea, during the latest Pleistocene to early Holocene. Quat. Res. 70 (2), 265–274. https://doi.org/10.1016/j.yqres.2008.04.014.

Litt, T., Brauer, A., Goslar, T., Merkt, J., Bałaga, K., Müller, H., Ralska-Jasiewiczowa, M., Stebich, M., Negendank, J.F., 2001. Correlation and synchronisation of Lateglacial continental sequences in northern central Europe based on annually laminated lacustrine sediments. Quat. Sci. Rev. 20 (11), 1233–1249. https://doi.org/10.1016/S0277-3791(00)00149-9.

Notebaert, B., Verstraeten, G., 2010. Sensitivity of West and Central European river systems to environmental changes during the Holocene: a review. Earth Sci. Rev. 103 (3), 163–182. https://doi.org/10.1016/j.earscirev.2010.09.009.

Paterson, G.A., Heslop, D., 2015. New methods for unmixing sediment grain size data. Geochem. Geophys. Geosyst. 16 (12), 4494–4506. https://doi.org/10.1002/2015GC006070.

Peng, F., Prins, M.A., Kasse, C., Cohen, K.M., Van der Putten, N., van der Lubbe, J., Toonen, W.H.J., van Balen, R.T., 2019. An improved method for paleoflood reconstruction and flooding phase identification, applied to the Meuse River in the Netherlands. Glob. Planet. Chang., 177, 213–224. doi:https://doi.org/10.1016/j.gloplacha.2019.04.006.

Phillips, J.D., 2010. Relative Importance of Intrinsic, Extrinsic, and Anthropic Factors in the Geomorphic Zonation of the Trinity River, Texas. Journal of the American Water Resources Association 46 (4), 807–823. https://doi.org/10.1111/j.1093-474X.2010.00457.x.

Pierik, H.J., Stouthamer, E., Cohen, K.M., 2017. Natural levee evolution in the Rhine-Meuse delta, the Netherlands, during the first millennium CE. Geomorphology 295, 215–234. https://doi.org/10.1016/j.geomorph.2017.07.003.

Prins, M.A., Vriend, M., Nugteren, G., Vandenberghe, J., Lu, H., Zheng, H., Jan Weltje, G., 2007. Late Quaternary aeolian dust input variability on the Chinese Loess Plateau: inferences from unmixing of loess grain size records. Quat. Sci. Rev. 26 (1), 230–242. https://doi.org/10.1016/j.quascirev.2006.07.002.

Reimer, P.J., Bard, E., Bayliss, A., Beck, J.W., Blackwell, P.G., Ramsey, C.B., Buck, C.E., Cheng, H., Edwards, R.L., Friedrich, M., Grootes, P.M., Guilderson, T.P., Haflidason, H., Hajdas, I., Hatté, C., Heaton, T.J., Hoffmann, D.L., Hogg, A.G., Hughen, K.A., Kaiser, K.F., Kromer, B., Manning, S.W., Niu, M., Reimer, R.W., Richards, D.A., Scott, E.M., Southon, J.R., Staff, R.A., Turney, C.S.M., van der Plicht, J., 2013. IntCal13 and Marine13 radiocarbon age calibration curves 0–50,000 years cal BP. Radiocarbon, 55(4), 1869–1887. doi: https://doi.org/10.2458/azu_js_rc.55.16947.

Ruijters, M.H.P.M., van Dijk, X.C.C., Ellenkamp, G.R., Tichelman, G., 2017. Afgedekte ruggen opgezocht. Onderzoeksgebied Ooijen-Wanssum in de gemeenten Venray en Horst aan de Maas; archeologisch vooronderzoek: een proefsleuvenonderzoek. Rapport-3153, the Netherlands.

Santisteban, J.I., Mediavilla, R., López-Pamo, E., Dabrio, C.J., Zapata, M.B.R., García, M.J.G., Castaño, S., Martínez-Alfaro, P.E., 2004. Loss on ignition: a qualitative or quantitative method for organic matter and carbonate mineral content in sediments? J. Paleolimnol. 32 (3), 287–299. https://doi.org/10.1023/B:JOPL.0000042999.30131.5b.

Smith, N.D., Cross, T.A., Dufficy, J.P., Clough, S.R., 1989. Anatomy of an avulsion. Sedimentology 36 (1), 1–23. https://doi.org/10.1111/j.1365-3091.1989.tb00817.x.

Tebbens, L.A., Veldkamp, A., Westerhoff, W., Kroonenberg, S.B., 1999. Fluvial incision and channel downcutting as a response to Late-glacial and Early Holocene climate change: the lower reach of the River Meuse (Maas), The Netherlands. Journal of Quaternary Science 14 (1), 59–75. https://doi.org/10.1002/(SICI)1099-1417(199902)14:1%3C59::AID-JQS408%3E3.0.CO;2-Z.

Thompson, R., Battarbee, R.W., O'Sullivan, P.E., Oldfield, F., 1975. Magnetic susceptibility of lake sediments. Limnol. Oceanogr. 20 (5), 687–698. https://doi.org/10.4319/lo.1975.20.5.0687.

Tipping, R., Davies, A., McCulloch, R., Tisdall, E., 2008. Response to late Bronze Age climate change of farming communities in north east Scotland. J. Archaeol. Sci. 35 (8), 2379–2386. https://doi.org/10.1016/j.jas.2008.03.008.

Toonen, W.H.J., Winkels, T.G., Cohen, K.M., Prins, M.A., Middelkoop, H., 2015. Lower Rhine historical flood magnitudes of the last 450 years reproduced from grain size measurements of flood deposits using End Member Modelling. CATENA 130, 69–81. https://doi.org/10.1016/j.catena.2014.12.004.

Toonen, W.H.J., Foulds, S.A., Macklin, M.G., Lewin, J., 2017. Events, episodes, and phases: Signal from noise in flood-sediment archives. Geology 45 (4), 331–334. https://doi.org/10.1130/G38540.1.

Törnqvist, T.E., Bridge, J.S., 2002. Spatial variation of overbank aggradation rate and its influence on avulsion frequency. Sedimentology 49 (5), 891–905. https://doi.org/10.1046/j.1365-3091.2002.00478.x.

Van Balen, R.T., Houtgast, R.F., Cloetingh, S.A.P.L., 2005. Neotectonics of The Netherlands: a review. Quat. Sci. Rev. 24 (3), 439–454. https://doi.org/10.1016/j.quascirev.2004.01.011.

Van den Bos, V., Engels, S., Bohncke, S.J.P., Cerli, C., Jansen, B., Kalbitz, K., Peterse, F., Renssen, H., Sachse, D., 2018. Late Holocene changes in vegetation and atmospheric circulation at Lake Uddelermeer (The Netherlands) reconstructed using lipid biomarkers and compound-specific δD analysis. J. Quat. Sci. 33 (1), 100–111. https://doi.org/10.1002/jqs.3006.

Van Geel, B., Buurman, J., Waterbolk, H.T., 1996. Archaeological and palaeoecological indications of an abrupt climate change in The Netherlands, and evidence for climatological teleconnections around 2650 BP. J. Quat. Sci. 11 (6), 451–460. https://doi.org/10.1002/(SICI)1099-1417(199611/12)11:6%3C451::AID-JQS275%3E3.0.CO;2-9.

Van Hateren, J.A., Prins, M.A., van Balen, R.T., 2018. On the genetically meaningful decomposition of grain size distributions: a comparison of different end-member modelling algorithms. Sediment. Geol. 375, 49–71. https://doi.org/10.1016/j.sedgeo.2017.12.003.

Vandenberghe, J., Lu, H., Sun, D., van Huissteden, J., Konert, M., 2004. The late Miocene and Pliocene climate in East Asia as recorded by grain size and magnetic susceptibility of the Red Clay deposits (Chinese Loess Plateau). Palaeogeogr. Palaeoclimatol. Palaeoecol. 204 (3), 239–255. https://doi.org/10.1016/S0031-0182(03)00729-6.

Ward, P.J., Renssen, H., Aerts, J.C.J.H., van Balen, R.T., Vandenberghe, J., 2008. Strong increases in flood frequency and discharge of the River Meuse over the late Holocene: impacts of long-term anthropogenic land use change and climate variability. Hydrol. Earth Syst. Sci. 12 (1), 159–175. https://doi.org/10.5194/hess-12-159-2008.

Ward, P.J., van Balen, R.T., Verstraeten, G., Renssen, H., Vandenberghe, J., 2009. The impact of land use and climate change on late Holocene and future suspended sediment yield of the Meuse catchment. Geomorphology 103 (3), 389–400. https://doi.org/10.1016/j.geomorph.2008.07.006.

Weltje, G.J., Prins, M.A., 2003. Muddled or mixed? Inferring palaeoclimate from size distributions of deep-sea clastics. Sediment. Geol. 162 (1), 39–62. https://doi.org/10.1016/S0037-0738(03)00235-5.

Wolman, M.G., Leopold, L.B., 1957. River flood plains: Some observations on their formation. 282C, Washington, D.C.

Yang, D., Yu, G., Xie, Y., Zhan, D., Li, Z., 2000. Sedimentary records of large Holocene floods from the middle reaches of the Yellow River, China. Geomorphology 33 (1), 73–88. https://doi.org/10.1016/S0169-555X(99)00111-7.

Zhao, H., Liu, Z., Song, L., Wang, C., Li, S.-H., 2018. OSL dating of flood sediments in the North China Plain. Quat. Geochronol. 49, 101–107. https://doi.org/10.1016/j.quageo.2018.07.010.

Zuidhoff, F.S., Bos, J.A.A., 2011a. Landschap en vegetatie Lomm Hoogwatergeul fase II. In: D.A. Gerrets & R. de Leeuwe (rEd.), Rituelen aan de Maas. Lomm Hoogwatergeul fase II, een archeologische opgraving. ADC-rapport 2333, ADC Archeo Projecten, Amersfoort.

Zuidhoff, F.S., Bos, J.A.A., 2011b. Landschap en vegetatie. In: D.A. Gerrets & G.L. Williams (rEd.), Water en Vuur. Archeologisch proefsleuvenonderzoek en opgraving te Lomm Hoogwatergeul Fase III. ADC-rapport 2703, Amersfoort.

Zuidhoff, F.S., Huizer, J., 2015. De noordelijke Maasvallei door de eeuwen heen. Vijftienduizend jaar landschapsdynamiek tussen Roermond en Mook. Inventariserend archeologisch onderzoek 'Verkenning Plus' project Maasvallei voor vijftien deelgebieden. ADC-Report 3750, ADC Archeoprojecten, Amersfoort.